UNIVERSITÀ DEGLI STUDI DI PADOVA

Dipartimento di Fisica e Astronomia "Galileo Galilei"

Master Degree in Astrophysics and Cosmology

Final dissertation

Binary Black Holes in Nuclear Star Clusters:

Dynamics and Time Evolution

Thesis supervisor

Prof. Michela Mapelli

Thesis co-supervisor

Dr. Manuel Arca Sedda

Candidate

Daxal Hemendrakumar Mehta

Academic Year 2022/2023

Abstract

The goal of this thesis is to study hierarchical mergers of binary black holes in evolving nuclear star clusters. Nuclear star clusters are dense and heavy objects located at the center of galaxies. Their mass and density can go up to $10^8 M_\odot$ and $10^5 M_\odot/pc^3$. Such conditions prove excellent to study hierarchical mergers. We begin by modeling a nuclear star cluster that is growing by star cluster infall through dynamical friction. Our goal is an expression for NSC mass that is growing with time. From this mass, we can infer the size of the NSC. These two quantities are sufficient to derive the necessary physical properties like escape velocity and density. We then implement this model into the FASTCLUSTER code, intensively updating the code in the process. To simulate the phenomenon, we also create a black hole library that is forming in the star clusters. We run 12 different simulations, varying the mass of galaxies, type of galaxies, and initial population of black holes. We find that not all nuclear star cluster are excellent for hierarchical mergers. Small escape velocity in lighter nuclear star clusters and long dynamical timescales in heavier nuclear star clusters stops hierarchical mergers. We also find that changing the initial mass population of black holes from local black holes produced in the nuclear star cluster to migratory black holes originating in star clusters heavily alter the binary black hole dynamics inside. We find that only a few NSCs are capable of producing black holes with mass greater than $1000 M_\odot$. Finally, we compare our results with gravitational wave events to understand if our simulations are able to reproduce those events.

Acknowledgement

I am grateful to Michela Mapelli and Manuel Arca Sedda for introducing me to this exciting and growing field of black hole dynamics. They have patiently guided me through the project, providing many helpful insights, helped in sorting out any problems that I encountered, and encouraged me repeatedly.
I also thank the DEMOBLACK group for many discussion that directly and indirectly gave me many necessary pointers for my project. Their experience decreased many mistakes I could have made.
I also thank my family who supported me emotionally and financially through my masters in Italy. I am also grateful for my friends who made my time in Padova fun and worthwhile.

Contents

List of Figures

List of Tables

Useful Abbreviation

Term	Definition
BH	Black hole
BBH	Binary black hole
IMBH	Intermediate mass black hole
SMBH	Super massive black hole
MBH	Massive black hole
NSC	Nuclear star cluster
GC	Globular cluster
YMC	Young assive cluster
LVK	LIGO-Virgo-KAGRA
EM	Electromagnetic waves
GW	Gravitational waves
GWTC	GW transient catalog
CE	Common Envelope
MS	Main Sequence
HST	Hubble space telescope
t_{rep}	Replenishment time
t_{DF}	Dynamical friction time
t_{form}	Black hole formation time
t_{3bb}	Three body interaction time
t_{121}	Exchanges time
LL	Local BH in late galaxy
LML	Local and migratory BH in Late galaxy
LME	Local and migratory BH in Early galaxy

Table 1: List of Acronyms

Chapter 1

Introduction

In September 2015, a hundred year long search for gravitational waves (GW) gave results. The Laser Interferometer Gravitational-wave Observatory (LIGO) at Hannover and Livingston, US, detected a signal coming from the merger of two black holes (BHs), GW150914, (Abbott et al. [2016]). Since then, we have had almost a hundred GW detections, including the third gravitational waves transient catalog (GWTC-3 Abbott et al. [2021]). Binary black holes (BBHs) contribute to most of these observations.

These many observations of GW have raised many important questions. BBHs were thought to exists from a long time ago but GW150914 was the first direct proof of them. Along with the existence of BBHs, this observation confirmed that BBHs could merge within Hubble time. Typical BBHs have merging timescales much larger than the Hubble time. We shouldn't see any GW events in our time. GW observations have forced us to think of processes that could solve this problem. One possible solution may be common envelope. When an original binary evolves, Roche-lobe overflow may cause the donor's outer surface to envelope the binary. This common envelope can suck the binary's orbital energy, causing it to shrink to a radius that can merge within Hubble time. We will discuss this process in depth in chapter 2.

Many of the GW observations have BHs with mass greater than $20M_{\odot}$, which contradicted earlier observations of BHs through X-ray binaries that had masses less than $20M_{\odot}$. The X-ray observations were supported by theories that did not predict BHs of masses greater than $30M_{\odot}$. However, GW observations broke the norm, forcing us to revise the theories of stellar evolution. Supporting the change were observations of BHs in pair-instability mass gap, which we thought weren't possible. For massive stars that have helium core between the masses of $64M_{\odot}$ and $133M_{\odot}$, the photons inside the core are powerful enough to produce electron-positron pair. The runaway collapse of the core due to this process would disrupt the star in a violent event called pair-instability supernova, leaving no compact remnant behind. However, we have found observations with primary mass in this mass gap, GW190521 and GW191109_010717. There is some other mechanism for the formation of these BHs and also the formation of their binaries.

Maybe BBH merger itself is the phenomenon behind the formation of massive BHs. Many of the GW events like GW170823 and GW170729 have remnant BHs in the pair-instability mass gap. However, this possibility raises other questions like: how did a remnant BH from a merger form a binary and merge a second time within Hubble time? Where are BBH mergers so efficient? We will see in chapter 2 that Hierarchical merger, which is a consequence of dynamical formation of BBH, can be the answer to these questions. In special environment where density of stellar objects is extremely high like globular clusters (GCs) or nuclear star clusters (NSCs), stars and their remnants may interact with each other frequently, resulting in processes like collision, three-body interactions, and exchanges. BHs may similarly interact in these dense environment and form binaries. Under repeated interactions, these BBHs may compress, eventually merging. If the remnant BH is retained by the cluster after the merger, it may go through the same process again. This would not only explain the existence of heavier BHs but also them being merging again.

Among star clusters, NSCs prove more efficient in hierarchical mergers than GCs or young massive clusters (Mapelli et al. [2021]). NSCs are compact dense objects present at the center of galaxies. They are extremely heavy with masses reaching up to $10^8 M_\odot$ and number density reaching up to $10^5 pc^{-3}$. As we will see in chapter 2, such dense environments make it extremely easy for BHs to form a binary and eventually merge.

The formation and evolution of NSCs is still an active field of research. Observation of stellar age of NSCs have shown that stars of varying ages are found in NSCs (Walcher et al. [2005],Kacharov et al. [2018]). This suggests a long star formation history, boosting the in-situ star formation theory, where gas accretes onto the NSC. Observation of GCs around nucleated galaxies found that there is deficit of GCs near the center of these galaxies (Lotz et al. [2001],Capuzzo-Dolcetta and Mastrobuono-Battisti [2009]). This fact promoted another theory for NSC formation, the globular cluster migration theory. In chapter 3, we will discuss these theories in depth, eventually settling on globular cluster migration for the purpose of this thesis.

Globular cluster migration states that any star clusters near the center of galaxies would spiral in through dynamical friction (Tremaine et al. [1975]). It is to be noted that the only requirement for the scenario is for a cluster to be formed sufficiently close to the center of the galaxy, it does not need to be a GC. The terminology globular cluster migration remains for historical reasons. This is a complex process that depends on the mass and spatial distribution of the star clusters and on the host galaxies. N-body simulations were performed to observe this phenomenon (Arca-Sedda and Capuzzo-Dolcetta [2014]) and they formulated an analytical model that produces similar results. We will recreate this model in chapter 3 to extract physical properties like NSC mass, density, velocity dispersion, half-mass radius for our future analysis.

In this thesis, we are interested in studying hierarchical mergers (refer section 2.3) of BBHs in realistic NSCs. Recreating this process through N-body simulation is computationally expensive. For a single merger, we would have to take into effect the forces of the background stars in the cluster. Semi-analytic methods greatly reduces the computational cost, also giving us the freedom to explore the parameter space.

FASTCLUSTER (Mapelli et al. [2021]) is a semi-analytical population synthesis code that simulates hierarchical mergers. We will use it to simulate our interest. In chapter 4, we will review FASTCLUSTER, its initial condition, methodology, and what physics goes behind the process. We will also see the results of BBH mergers in unrealistic and non-evolving NSCs. In the paper introducing the code, they have found NSCs excellent for hierarchical mergers. But are all NSCs efficient? Does the formation channel of NSC affect the dynamics of BBHs inside? Does the evolution of NSC through accretion of mass change the dynamics of BBHs? These are the questions we will try to answer in this thesis.

To study these questions, we will need to introduce a realistic model of NSC into FASTCLUSTER. We will implement globular cluster migration scenario into FASTCLUSTER, changing the code deeply in the process. We will also need to create new BH libraries for our purpose. This will be discussed in chapter 5.

In chapter 6, we will see the result of our analysis. We indeed find that not all NSCs produce massive BHs beyond $1000 M_{\odot}$. Depending on the size and mass of the NSCs, we get different type of BH dynamics.

Chapter 2

Binary Black Holes

Stellar mass BHs form as the end results of stars and are some of the most exotic objects of the universe. They are characteristic of their strong gravitational field from which, even light cannot escape. In a BBH, two of these extreme objects interact through the exchange of energy and momentum, exhibiting phenomenon that can't be observed elsewhere. They emit GW, which causes them to spiral towards each other until they merge into a single more massive BH. BBH are of great interest to astrophysicists as they provide insights from stellar evolution to galaxy formation.

Physical properties of the binaries define the GW that are emitted. Conversely, we can say the GW carry away information regarding the binary. Thus, it becomes vital to study the properties of a binary that may affect its evolution and GW emission. BBH are characterized by the following properties:

- **Masses:** Mass play an important role in determining GW emission, the merging timescales, and even the remnant's state. We will suppose m_1 and m_2 to be the two BHs' masses with $m_1 \geqslant m_2$. Since they are in a binary, we will also define reduced mass for the system,

$$\mu = \frac{m_1 m_2}{M}, \tag{2.1}$$

  where $M = m_1 + m_2$ is the total mass of the system. Another important quantity is chirp mass of the system, defined as,

$$M_c = \mu^{3/5} M^{2/5}. \tag{2.2}$$

- **Semi-major axis (a):** The orbital separation between the masses define how long it will take to merge. In a cluster system, it will determine if a binary is strong enough to endure the interactions or not.

- **Eccentricity (e):** This quantity also defines how fast a merger will take place. If a binary is highly eccentric, it releases energy through GW much faster than a circular binary.

- **Spins:** Each BH has a spin, passed to them by their progenitor stars. We will call them $\vec{S}_1$ and $\vec{S}_2$. Their alignment with the orbital angular momentum greatly influences the evolution of the binary.

2.1 Formation Channels of Binary Black Holes

Isolated Formation

With more than fifty percent of current stars in binaries or higher order systems (Tian et al. [2018]), it is no surprise that we expect BHs to remain in binaries, albeit a smaller number. BBHs formed in such a way are called original binaries. In this section, we discuss some of the most important binary evolution processes.

Mass Transfer

If matter is exchanged between two stars of a binary, we call it mass transfer. It can happen either through stellar winds or Roche-lobe overflow. When a star loses mass through stellar winds, the companion may be able to capture some of the mass depending on the separation between them, the velocity of the wind, and the gravitational potential of the companion. Hurley et al. [2002] gave a nice expression to describe the accretion by stellar winds based on Bondi-Hoyle mechanism,

$$\dot{m}_2 = \frac{1}{\sqrt{1-e^2}}\left(\frac{Gm_2}{v_w^2}\right)^2 \frac{\alpha_w}{a^2}\frac{1}{[1+(v_{orb}/v_w)^2]^{3/2}}|\dot{m}_1|, \tag{2.3}$$

where e is the eccentricity of the binary, m_2 is the mass of the accretion star, v_w is the velocity of winds, $v_{orb} = \sqrt{G(m_1+m_2)/a}$ is the orbital velocity, $\alpha_w \sim 3/2$ is the efficiency constant, and $\dot{m}_1$ is the mass loss by the donor star through stellar winds. If we were to input the typical quantities of stellar winds ($\dot{m}_1 = 10^{-3} M_\odot/yr$ and $v_w = 1000 km/s$), we will find the mass accretion too low or inefficient. The companion receives an extremely small fraction of the mass lost by the donor.

Roche lobe overflow is a much better mechanism for mass transfer. Roche lobe is the region around a star where gravitational forces are balanced out by its companion. It is the maximum equi-potential surface where matter is bound to the star. Roche-lobe has a teardrop shape with the apex of teardrop located between the two bodies, also called the L_1 Lagrangian point. If matter of the first star exceeds the Roche lobe, it can fall-off to the companion via L_1 Lagrangian point. This process is called Roche lobe overflow. Mass transfer alters the binary's masses, changing masses and radius for both stars. If the mass loss in not conservative, the binary may lose angular momentum, affecting the semi-major axis.

As mass transfer begins, the donor's radius changes along with the Roche lobe's radius. If the Roche lobe compresses faster than the donor's radius, we can have unstable and runaway mass transfer, meaning that the mass transfer rate increases speedily. If the donor's core and envelope are clearly distinct, the binary can enter common envelope, where the donor's envelope surrounds both stars.

Common Envelope

When the binary enters the common envelope (CE) phase, the envelope stops rotating with the binary inside. For the binary, it is like suddenly moving in a dense medium. The gas causes a drag to the binary's rotation, sucking away energy from it. If the envelope uses this energy to expand end eventually eject, then we will get two naked stellar cores whose orbital separation is much smaller than the original binary. This ejection is crucial for the formation of BBHs whose orbital separation is small enough for them to merge within Hubble time.

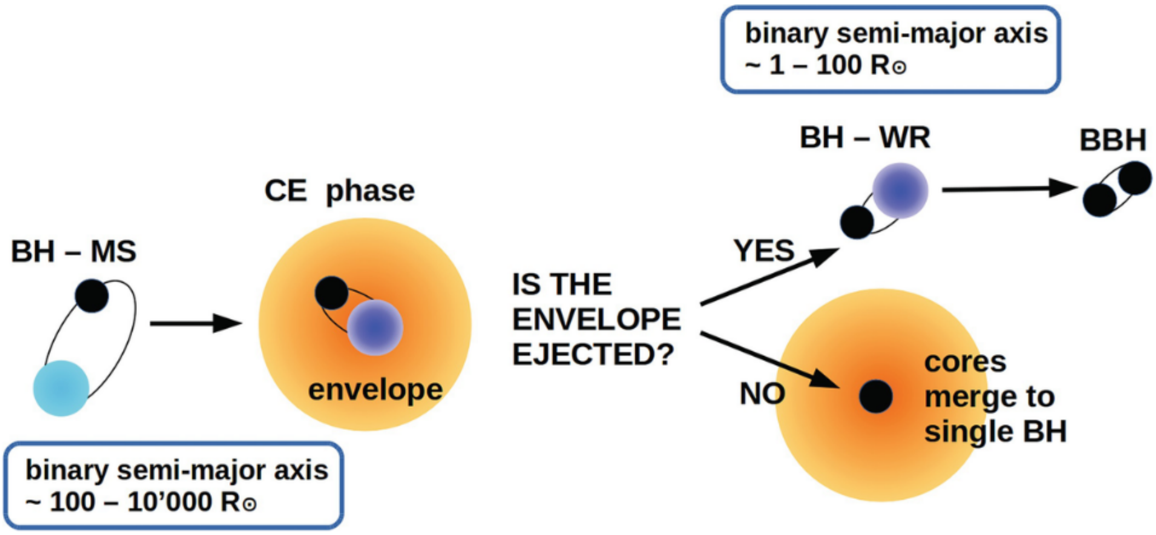

Figure 2.1: Common Envelop Scenario: A main sequence star is in binary with a BH. When the main sequence stars enters red giant phase, its outer radius can extend until it overfills the roche lobe and eventually form a common envelope around them. The core and BH spirals towards each other, giving energy to the CE. If the CE is ejected we can have a Wofl-Rayet star and BH binary that can eventually evolve to form a BBH. If the core is not ejected, the BH and core mergers in the CE before a BBH can form. (Mapelli [2020])

Conversely, if the envelope isn't ejected, it keeps extracting energy from the binary, causing the binary to prematurely merge in the end. The end result is a BH covered by an envelope.

We will use α formalism developed by Webbink [1984] to describe the common envelope. The basic concept is that the energy required to eject the envelope should be a fraction of the energy lost by the binary during inspiral.

$$\Delta E = \alpha(E_f - E_i) = \alpha \frac{G m_{c1} m_{c2}}{2}\left(\frac{1}{a_f} - \frac{1}{a_i}\right). \tag{2.4}$$

$m_{c1}(m_{c2})$ are the masses of the cores of primary(secondary) body. On the other hand, the binding energy of the envelope is,

$$E_{env} = \frac{G}{\lambda}\left[\frac{m_{env,1} m_1}{R_1} + \frac{m_{emv,2} m_2}{R_2}\right], \tag{2.5}$$

where $m_{env,1}(m_{env,2})$ is the envelope masses of the primary(secondary) member. λ is a parameters that captures the compactness of the envelope. The smaller λ is, the compact the envelope is and the more energy is needed to eject it. By forcing $\Delta E = E_{env}$, we can derive and expression for the final semi-major axis for which the envelope will be ejected. If a_f is smaller than the sum of the two core radii, it means the binary would merge before enough energy to expel the envelope is obtained. Conversely, if it is larger, the binary can survive. These surviving cores can evolve to form BHs.

The physics behind CE is much more complex than what we have discussed here. We haven't considered radiation pressure, nuclear energy, tidal effects. Nevertheless, we now have a general idea of how isolated binaries evolve to BBH.

Dynamical Formation

Most of the stellar binaries we observe have large semi-major axis for GW emission to have any impact. The coalescence time, which is the time taken by a binary to merge from GW emission can be calculated according to the following equation (refer Appendix A),

$$\tau = \frac{5}{256}\frac{c^5 R^4}{G^3 M^2 \mu}, \tag{2.6}$$

where R is the orbital separation or semi-major axis of the binary, M is their total mass, and μ is their reduced mass. For a separation of $10AU$ and BBHs of $10M_\odot$ each, we get coalescence time in the range of,

$$\tau \approx 10^{18} yr \left(\frac{R}{10AU}\right)^4 \left(\frac{20M_\odot}{M}\right)^2 \left(\frac{10M_\odot}{\mu}\right). \tag{2.7}$$

If all the binaries in the universe were separated with semi-major axis larger than a few AU, we won't receive GW within our time unless some mechanism shortens the semi-major axis below $1AU$. This was known as the final AU (Stone et al. [2017]). As we saw in the above section, CE is one of the solutions. CE helps in shortening the semi-major axis with it taking away a fraction of the binary's energy. We will now discuss another possible mechanism, called the dynamical channel.

Dynamical channel only becomes prominent in dense systems where the density of stellar bodies go above $10^3 pc^{-3}$. Such densities can easily be achieved in star clusters. Star clusters are also locations for the birth of massive stars that can be progenitors of BHs. As such, we expect a significant population of BHs to be present in star clusters. There are several types of star clusters:

- Globular cluster are old, heavy, with high densities. They can have $10^4 - 10^6$ stars with number density going up to 10^5 near the center. They have long lifetime and can form along the galaxy. A fraction of the galaxy's baryonic mass is within these clusters.
- Young massive clusters (YMC) are characterized by intense star formation episodes. They are also stellar nurseries for massive stars. They have masses around $10^4 M_\odot$ and number density at $10^3 pc^{-3}$. They are short lived, often disrupted by the galaxy's tidal effect, releasing stars in the galaxy plane or field. If they survive the tidal disruption, they may evolve to open clusters.
- Nuclear Star Clusters are the heaviest star clusters with their mass going up to $10^8 - 10^9 M_\odot$. We will discuss more of their properties in the next chapter.

Lastly, we can also have dynamical formation in the accretion disk around a supermassive black hole (SMBH), where it is not the stars that influence the dynamics but the disk.

The main driving force behind the dynamics of stars is gravity. We can distinguish these interactions in the following ways:

Three Body Interactions

In star clusters, it is possible for three bodies to interact with one taking away the kinetic energy of the system. The remaining two bodies gets bound in a binary, whose orbital separation depends on their initial conditions and ejected energy. For a star of mass m, its cross scattering area due to gravity is,

$$\sigma_{cs} = \pi b^2, \tag{2.8}$$

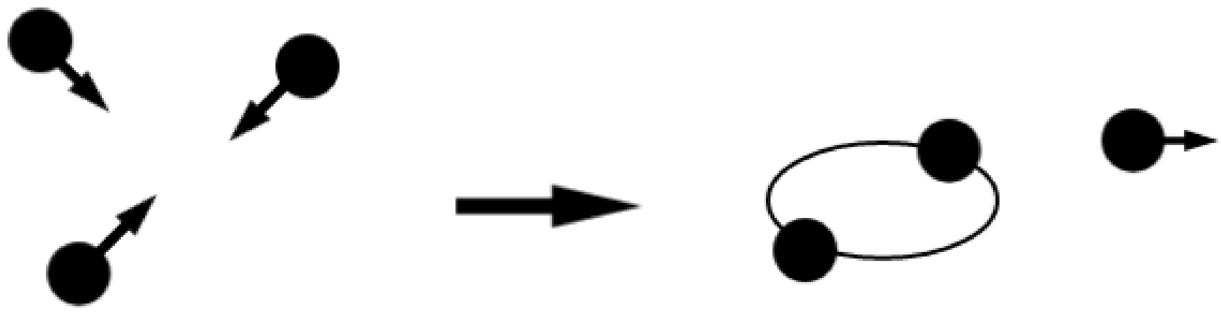

Figure 2.2: Three single stars can come close enough to each other and interact. The smallest mass will carry away majority of the kinetic energy and get ejected from the cluster. The remaining two will form a binary.

where b is the impact parameter, the distance at which gravitational forces significantly alter the path of the star. Impact parameter depends on the mass and velocity of the star. If the velocity dispersion of the cluster is v and density of stellar bodies in the environment is n, the interaction rate between two bodies is given by $n\sigma_{cs}v$. For a third body to interact with these two, it should be within a volume around them, which can be shown by nb^3. Thus, for a cluster with N stellar bodies, their rate of interactions is given by λ,

$$\begin{aligned}\lambda &= Nn^2\sigma_{cs}vb^3 \\ &= \pi Nn^2vb^5.\end{aligned} \tag{2.9}$$

Impact parameter, b, can be written as $2Gm/v^2$, giving us

$$\lambda = \frac{32\pi Nn^2G^5m^5}{v^9} \tag{2.10}$$

Inverting this expression gives us the timescales on which a star of mass m can form a binary through three body interactions.

$$t_{3b} = \frac{v^9}{32\pi Nn^2G^5m^5}. \tag{2.11}$$

An important parameter to notice here is the dependence of three-body timescales on velocity dispersion of the cluster. A small increment in the velocity may heavily alter the time taken to form a binary. On the contrary, the heavier the star is, the less time it takes to form a binary, owing to its greater gravitational force. If we insert the characteristic values for physical properties of a cluster in equation 2.10, we get an estimate on how frequently such interactions occurs within a cluster. For a cluster with 10^6 bodies, its number density goes like 10^5 and velocity dispersion is in the range of $\sim 30Km/s$. A star with mass of $10M_\odot$ will form binary in,

$$t_{3b} = 152Myr\left(\frac{v}{30Km/s}\right)^9\left(\frac{10^6}{N}\right)\left(\frac{10^5pc^{-3}}{n}\right)^2\left(\frac{10M_\odot}{m}\right)^5 \tag{2.12}$$

Within just 152 million year after the star forms in a dense cluster, it can enter a binary. It can be seen that an increase in velocity dispersion by a factor of two or $v = 60Km/s$ results in the three-body time to increase to 77.8 billion years. Conversely, an increase in mass of the star by a factor of two, $m = 20M_\odot$, the time decreased to 4.75 million years. These two factors will play an important role when we will discuss the dynamics of BBHs in different NSCs. The binary formed after this time would be hard, it won't be disrupted by other stars in the cluster.

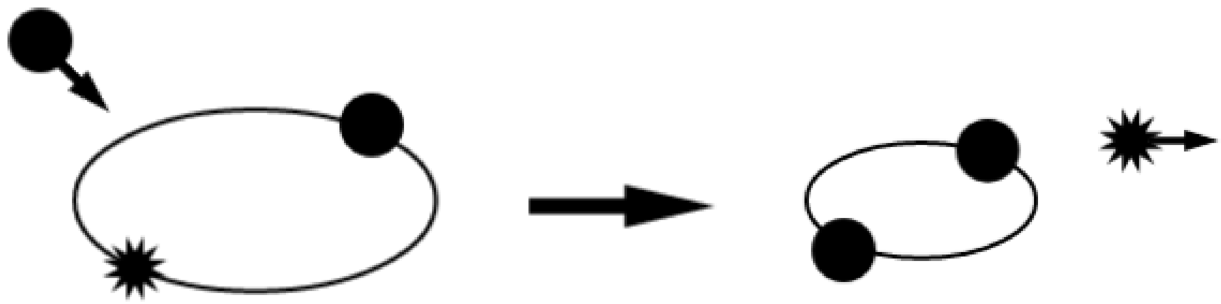

Figure 2.3: When a BH with mass m_3 approached a binary that is soft with $m_3 > m_2$ and $m_1 > m_2$, it can kick the lighter mass, m_2 , from the binary. m_2 will carry away the initial kinetic energy of the heavier mass, getting ejected from the cluster

Exchanges

We have discussed how single stars would form binaries but a fraction of stellar bodies start their lives as binaries. These original binaries may be soft, meaning they can be disrupted by the dynamics of the cluster. A heavier body can knock the lighter body of the binary and take its place. This process favors the formation of heavier binaries, which are harder. Such interactions may completely disrupt the binary too. This can be determined by comparing the binding energy of the binary to the average kinetic energy of the cluster. If the velocity dispersion of the cluster is v, the orbital separation of the binary must be smaller than $a = 2GM/v^2$ for it to survive an average interaction. Otherwise the binary would get disrupted. We will derive an timescale estimate like we did before to understand this process well. The calculation would deviate a little, owing to the consideration of a binary. The cross section we take this time is the area of the binary.

We can consider the binary as a single body, which greatly eases the calculation. The rate of interaction is given by $nv\sigma_{cs}$, so the timescales of exchanges are,

$$t_{12} = \frac{1}{nv\sigma_{cs}} \tag{2.13}$$

The cross section for such interactions is,

$$\sigma_{cs} = 4\sqrt{\pi}(a^2 + ab), \tag{2.14}$$

where a is the semi-major axis and b is the impact parameter. The impact parameter also differs from the three body case since we consider the gravitational effect of the binary with a third body. $b = GM_{123}/v^2$, where $M_{123} = 2m + m_b$. Here, m is the average mass of stellar bodies in the cluster while m_b is the BH for which we are calculating the timescale. For hard binaries, the semi-major axis is usually small, which causes the second term in equation 2.14 to dominate. So, the exchange timescale can be simplified to,

$$\begin{aligned} t_{12} &= \frac{1}{4\sqrt{\pi}nvab} \\ &= \frac{v}{4\sqrt{\pi}GM_{123}na}. \end{aligned} \tag{2.15}$$

The average mass of stellar bodies in clusters can be taken as $1M_{\odot}$. For a BH of mass $10M_{\odot}$, semi-major axis of 1AU, and similar cluster properties as the three body case, we arrive at the expression,

$$t_{12} = 180Myr\left(\frac{v}{30Km/s}\right)\left(\frac{12M_{\odot}}{M_{123}}\right)\left(\frac{10^5pc^{-3}}{n}\right)\left(\frac{1AU}{a}\right). \tag{2.16}$$

For these values, exchange timescales are similar to three body timescales. This won't necessarily be true for different parameter values. Exchange timescales is not heavily dependent on velocity dispersion and mass. A further addition to this simplification is to consider the fraction of stellar bodies within the cluster that are in binaries. This may change the timescales by an order too.

During an exchange scenario, the binary may harden by giving energy to the ejected body. By conservation of energy, this kinetic energy comes from the binary's binding energy. The binary recoils by conservation of momentum. If this recoil velocity is larger than the escape velocity of the cluster, even the binary may escape. After the binary is ejected from the cluster, its orbital evolution only depends on GW emission. As we have seen, depending on the semi-major, we may never get to observe the merger of binaries that were ejected.

We can derive an expression for the semi-major axis that will eject the binary. On average, an exchange would decrease the semi-major axis by a factor of 7/9 (Kocsis [2022]), which we will call δ. We can calculate the difference in energy brought my this,

$$\begin{aligned}\Delta E &= -\frac{Gm_1m_2}{a} - \left(-\frac{Gm_1m_2}{7a/9}\right)\\ &= \frac{Gm_1m_2}{a}\left(\frac{1}{\delta} - 1\right).\end{aligned} \tag{2.17}$$

In our case, $m_1 = m_2 = m$. This energy is carried by the binary and the third body.

$$\Delta E = \frac{1}{2}(2m)v_{bin}^2 + \frac{1}{2}m_3v_3^2 \tag{2.18}$$

From conservation of momentum, we also have

$$2mv_{bin} + m_3v_3 = 0 \tag{2.19}$$

Substituting $v_3 = -2m_{bin}/m_3$ in equation 2.18, we compare it with equation 2.17. For the binary to be ejected from the cluster $v_{bin} \geqslant v_{esc}$, so we get an expression,

$$a_{ej} = \left(\frac{1}{\delta} - 1\right)\frac{mm_3}{(2m + m_3)}\frac{G}{v_{esc}^2} \tag{2.20}$$

For all three bodies with mass $10M_{\odot}$ and escape velocity of $30Km/s$, we get the semi-major axis value,

$$a_{ej} = 0.36AU\left(\frac{m}{10M_{\odot}}\right)\left(\frac{30Km/s}{v_{esc}}\right)^2 \tag{2.21}$$

A binary whose total mass is $20M_{\odot}$ will get ejected by interacting with a BH of mass $10M_{\odot}$ if its semi-major axis is smaller than $0.36AU$. If escape velocity of the cluster increases, the semi-major axis decreases, making it harder for the binaries to be ejected by recoil. Binaries can harder more in heavier clusters.

Dynamical Friction

When a massive BH moves in dense clusters, it gets influenced by the background field of stars, causing it to lose kinetic energy. This process is called dynamical friction and causes the BH to inspiral towards the depth of the potential well, which is the star cluster's center. Due to stellar bodies infalling towards the core of the cluster, the central density is greater than the cluster. According to equations [2.12], [2.16], the increase in density decreases the timescales, making three-body interactions and exchanges more efficient. BHs in the core form binaries more quickly than elsewhere in the cluster.

Chandrasekhar [1943] gave us the drag felt by a star of mass M, moving through a homogeneous ocean of stars,

$$\frac{dv}{dt} = \frac{4\pi G^2 M}{v^2}\rho \ln \Lambda, \tag{2.22}$$

where ρ is the density of stars. Λ is called Coulomb logarithm and is the ratio between the maximum and minimum impact parameter for the star. (For our application, we will take $\ln \Lambda$ as 10). The heavier a star is, the more drag force it will experience. If the star is moving with higher velocities, it will experience less drag. Inverting this equation can give us an idea on what timescales would this star inspiral to the core,

$$t_{DF} = \frac{1}{4\pi G^2 \ln \Lambda}\frac{v^3}{M\rho} \tag{2.23}$$

For typical values in a star cluster, this comes out to be,

$$t_{DF} = 11.25Myr\left(\frac{v}{30Km/s}\right)^3\left(\frac{10M_\odot}{M}\right)\left(\frac{10^5 M_\odot/pc^3}{\rho}\right). \tag{2.24}$$

Equations 2.22 and 2.23 can be applied to a multitude of cases in astrophysics. They define the friction a star cluster feels inside the galaxy, which may spiral into the NSC. They can also explain the inspiral of galaxies in large galaxy clusters.

In calculating three-body timescales, exchange timescales, and dynamical friction timescales, we have kept the cluster properties and BH mass constant and typical. Comparing the three timescales give us an idea what might occur in the cluster. If a BH forms at the edges of a star cluster and we assume that all dynamical processes begin at once, dynamical friction will take the shortest time. The BH is brought to the core before it forms a binary. It is safe to assume that most of the BHs form hard binaries when they reach the core. This fact is assumed in creating the FASTCLUSTER code, which we will discuss in Chapter 4.

2.2 Dynamical Evolution of Binary Black Holes

Heggie [1975] showed us that in star clusters, soft binaries will go softer while hard binaries will go harder. All the future interactions will only take away energy of the binary and help them merge in a process called 'Hardening'. We will now discuss the changes hardening brings to the orbit of a BBH. If a third body comes near the binary and extracts internal energy, it will cause the kinetic energy to increase and binding energy to decrease,

$$E_{b,f} = \frac{Gm_1m_2}{a_f} > \frac{Gm_1m_2}{a_i} = E_{b,i}, \tag{2.25}$$

which implies that $a_f < a_i$ if the masses are conserved. The binary shrunk when as a consequence to the third body passing by. For our work, we will derive the cumulative effect of hardening from the entire cluster on the binary like we have done in the previous section.

The cross section for a three body encounter is,

$$\sigma = \pi b_{max}^2, \tag{2.26}$$

where b_{max} is the maximum impact parameter the third body can have to influence the binary, i.e. exchange of energy is not zero. Under the assumptions that the binary is hard and the exchange of energy is significant ($b_{max} \sim a$), we can rewrite the above equation as,

$$\sigma = \pi b_{max} a = \frac{2\pi G(m_1 + m_2 + m_3)a}{v^2}, \tag{2.27}$$

where we have used the fact that b can be written as $2Gm/v^2$. Similar to our discussion for exchanges, the rate of interactions is given by $nv\sigma$ or explicitly,

$$\frac{dN}{dt} = nv\sigma = \frac{2\pi G(m_1 + m_2 + m_3)na}{v} \tag{2.28}$$

We are interested in finding the energy change brought by these interactions. We will combine the above equations with results of Hills [1983]. Using their numerical simulations, we can write the average change in binary energy per encounter is,

$$< \Delta E_b >= \xi \frac{m_3}{m_1 + m_2} E_b. \tag{2.29}$$

ξ is a post encounter energy parameter that can estimate to $\sim 0.2 - 1$ from numerical simulations (Quinlan [1996]). It can be seen from the above expression that for binary with large binding energy, their loss would also be great, which is Heggie law written in mathematically expression: hard binary will tend to harden. The above expression has been derived under three assumptions: the binary should be hard, the third body should pass close by ($b \lesssim 2a$), the mass of the third body shouldn't be greater than the binary $m_1 + m_2 >> m_3$. Now, we can combine equation 2.28 and 2.29 to write,

$$\frac{dE_b}{dt} =< \Delta E_b > \frac{dN}{dt} = \frac{\pi \xi G^2 m_1 m_2 \rho}{v}, \tag{2.30}$$

where $\rho = n < m >$, the average mass of the cluster mass (similar to what we did in exchanges). We can translate the above expression in semi-major axis a using equation 2.25,

$$\frac{da}{dt} = -2\pi\xi \frac{G\rho}{v} a^2, \tag{2.31}$$

The change is coherent with what we saw earlier. The greater the density, the more faster they will merge and opposite can be said for velocity dispersion.

As the semi-major axis becomes smaller and smaller, so does the cross section for hardening. It will become inefficient below a certain a and GW emission will take over the semi-major axis evolution. Peters [1964] gave us the change in semi-major axis as GW takes away the energy,

$$\frac{da}{dt} = -\frac{64}{5} \frac{G^3 m_1 m_2 (m_1 + m_2)}{c^5 a^3 (1 - e^2)^{7/2}} f_1(e), \tag{2.32}$$

where e is eccentricity, $f_1(e) = 1 + \frac{73e^2}{24} + \frac{37e^4}{96}$. We can write the combined equation for semi-major axis's evolution as,

$$\frac{da}{dt} = -2\pi\xi\frac{G\rho}{v}a^2 - \frac{64}{5}\frac{G^3 m_1 m_2(m_1+m_2)}{c^5 a^3(1-e^2)^{7/2}}f_1(e), \tag{2.33}$$

We know that as semi-major axis decreases, hardening becomes inefficient while GW becomes stronger. From the above expression, we can derive the precise a at which GW takes over hardening by equating the two sides,

$$a_{GW} = \left[\frac{32G^2}{5\xi c^5}\frac{v m_1 m_2(m_1+m_2)}{\rho(1-e^2)^{7/2}}f_1(e)\right]^{1/5} \tag{2.34}$$

For all $a \geqslant a_{GW}$, the semi-major axis shrinks due to hardening while for $a \leqslant a_{GW}$, GW emission shapes the binary. We can compare this expression to equation 2.21 to find an important condition for the binary to merge within the cluster. If $a_{ej} > a_{GW}$, it will be ejected by three-body interactions before GW can take over, causing this binary to merge outside the cluster on a much longer timescale.

Eccentricity of the binary similarly evolves through the two processes,

$$\frac{de}{dt} = 2\pi\xi\kappa\frac{G\rho}{v}a - \frac{304}{15}e\frac{G^3 m_1 m_2(m_1+m_2)}{c^5 a^4(1-e^2)^{5/2}}f_2(e), \tag{2.35}$$

where $\kappa \equiv \frac{de}{d\ln(1/a)}$, defined in Quinlan [1996]. Together with the semi-major axis equation, these two equations govern the binary's evolution. The coalescence time with eccentricity will add a term in equation 2.6

$$\tau = \frac{5}{256}\frac{a^4 c^5}{G^3 m_1 m_2 M}\frac{(1-e^2)^{7/2}}{f_1(e)} \tag{2.36}$$

Binaries with higher eccentricities have shorter coalescence times.

2.3 Hierarchical Mergers

I will present the summary of this chapter considering the life of one BH in a star cluster.

A star forms randomly in the cluster. The homogeneous sea of background stars affect the star's motion as it spirals towards the cluster's core. Suppose that this star has a mass that will surely cause it to end up as a BH. Depending on this mass and metallicity, this star may turn to BH along the journey to the core or it may turn afterwards in the core. Whenever it turns, the BH will receive a supernova kick, which will once again throw it towards the outskirts of the cluster.

The BH is similarly affected by the homogeneous background, inspiraling towards the core. When it reaches the core, its environment is so dense that now other stellar bodies (BH from now) are no longer background. They can directly interact with our BH, changing its velocity and direction by a significant factor. At an instance, our BH is hurling towards two other BHs. The three BHs interact and the lightest BH bears the brunt. It is thrown away by the remaining two, our BH now has a companion. It has just begun a stable orbit with its companion when an intruder comes and completely destroy our BH's binary. All three BHs are thrown away. After many such interactions, our BH finally manages to form binary with a companion. The

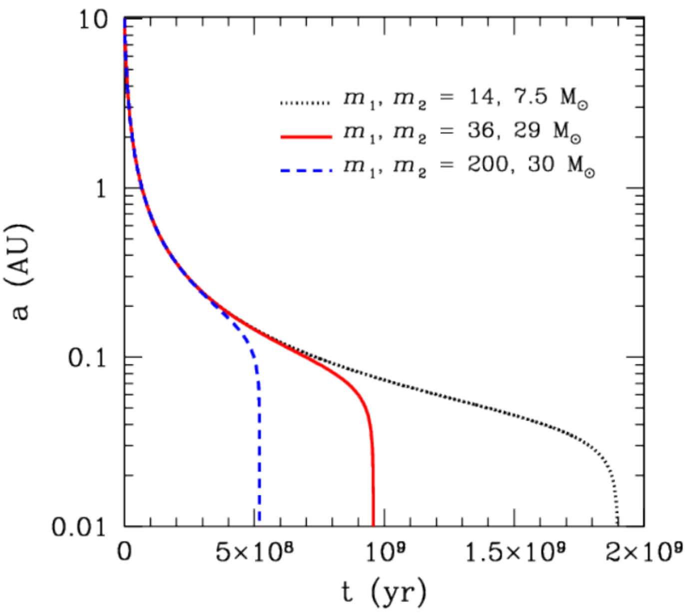

Figure 2.4: Evolution of semi-major axis with time for three different mass binaries. Massive binaries take shorter time to merge, a result of equation 2.33. When semi-major axis is large, the evolution curves of all three binaries are same due to hardening, which only depends on the cluster properties. When $a \sim a_{GW}$, GW begins to dominates and separates the evolution tracks according to the masses. Image credit:Mapelli [2020]

binary is hard and now, all these interactions no longer threatens its existence. Instead, they only help the binary become more harder until the force of gravity becomes too strong.

Ripples in the fabric of space-time spreads at the expense of the binary's energy. The loss through GW only increases with time until the BHs merge in a violent explosion of GW. Almost ten percent of the binary's total mass is converted to GW that spread across the universe. The remnant BH is now around ninety percent of the binary's mass and receives a relativistic kick from the merger. Fortunately, the force of this kick was unable to completely remove it from the cluster. It is now just a heavier BH that can retrace the footsteps of its progenitor.

The phenomenon of one BH merging several time is called Hierarchical mergers. This scenario is what we study in this thesis. FASTCLUSTER, which we will see in chapter 4, is based on such logic.

Chapter 3

Nuclear Star Cluster

Nuclear Star Cluster are dense compact objects present at the center of galaxies. For a long time, it was known that central regions of galaxies manifested a surface brightness peak, regardless of their morphological type. Limiting the study of this phenomenon was our inability to resolve the source and disentangle the compact nucleus from the galaxy's density profile. Fortunately, as techniques and telescopes advanced, we were able to prove that nuclear stellar clusters were indeed a separate feature of the galaxy. It was first shown in M31 by Light et al. [1974] since dust prevented us from observing Milky Way's center.

With advancement in telescopes, particularly the breakthroughs brought by Hubble Space telescope (HST), the study of NSC received attention from both theorist and observational people. In section one, we will see the properties deduced from observations. Based on the properties, we will theorize some scaling relations and formation channels for NSC in section 2 and 3. In section 4 and 5, we will briefly discuss the dynamics inside a cluster and the presence of SMBH. Finally, in section 6, we will create a semi-analytical model for the globular cluster migration scenario.

3.1 Properties of NSC

With the last two decades of observations, we have been able to deduce the following properties of NSC.

- **Size:** Due to their location and environment, it is not easy to determine the sizes of NSCs. HST was only able to resolve the closest NSCs to us. We define effective radius r_{eff} as the radius that contains half of the NSC's light. Through observations, we have found the median of r_{eff} to be around $3.3^{+7.0}_{1.9}pc$, which is comparable to globular clusters. Although, we have a longer tail in NSC, going up to $30 - 40pc$. If we use Dehnen density profile to explain the galaxy's density, we can translate effective radius to the half-mass radius using a simple equation: $r_{hm} = (4/3) * r_{eff}$ (Dehnen [1993]). For our analysis, we will find the half-mass radius more functional. NSC also shows non-spherical characteristics, with eccentricities going as high as 0.6. In Late-type galaxies, the NSCs also exhibit a flattened shape. Their shape scales with the host galaxies and may prove to be a constraint towards their formation mechanism.

- **Luminosity and Mass:** NSCs are very luminous objects and are sometimes hard to directly distinguish them from the galaxy's central luminosity. We need sophisticated methods to find their luminosity. From their brightness, we can extract their stellar masses using relations of color and mass-to-light ratio for stellar populations. We can

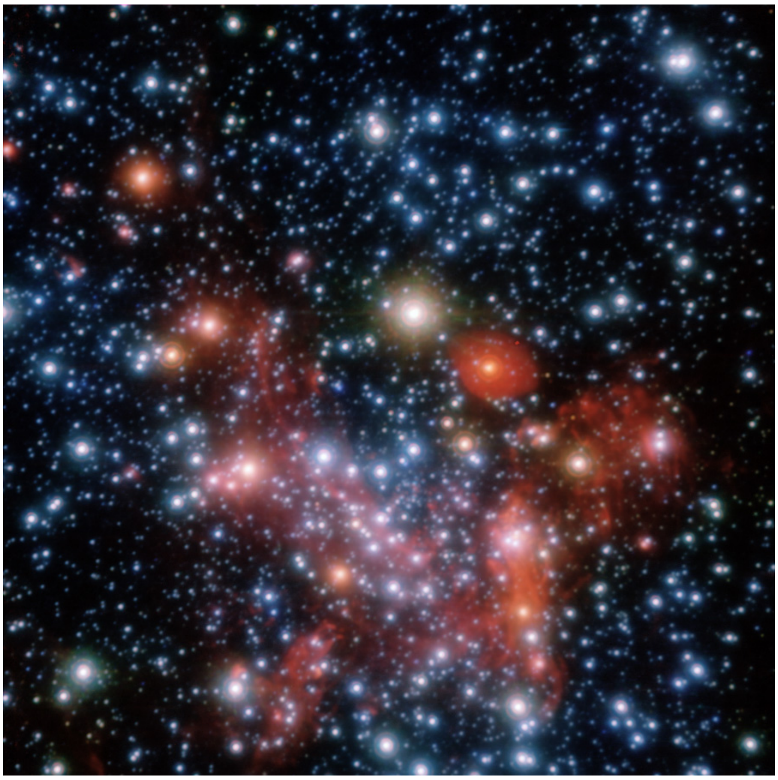

Figure 3.1: NSC in the center of Milky Way. The image is taken in infrared using the NaCo instrument on VLT. Image Credit Stefan Gillessen, Reinhard Genzel, Frank Eisenhauer (ESO).

also use spectroscopic and dynamical approaches to measure their masses. We found that NSC have masses ranging from $10^5 - 10^9 M_{\odot}$ with the distribution peaking at $10^{6.5} M_{\odot}$.

- **Density:** From the above discussed mass and radius, we can already estimate that NSCs are extremely dense objects. From the observed data, we can make a few conclusions: i) For NSCs of mass lower than $10^6 M_{\odot}$, the radius is independent on mass while beyond that, the radius increases proportional to mass. The quantities change is such a way that the surface density is preserved. ii) For a NSC of same mass, the NSCs in late-type galaxies are more compact than in early-type galaxies. (We will use this fact in our simulation later.) iii) The most massive NSCs can go up to $10^6 M_{\odot}/pc^2$ in surface density. Central volume densities in NSCs are also within the same range, going even up to $10^7 M_{\odot}/pc^3$ in our Milky Way.

- **Age and Metallicity:** If we could resolve individual stars in an NSC, it becomes easy to measure the age and metallicity. Unfortunately, this is only possible for the nearest NSCs. For others, we have to fit their integrated light to find the stellar population. In the integrated light, we can easily determine the young stars population as they dominate the light. But it is difficult for the old population. The latter is important since they can tell us when the NSC was formed.

  In late-type galaxies, we find that the data prefers an extended history of star formation rather than a single stellar population. Although the older population dominates the NSCs, we also find stars younger than a 100 Myr, suggesting a recent burst in star formation. The presence of these younger generation stars prefers the in-situ formation model for NSC. These younger generation stars are more concentrated at the center of

NSCs.

In early-type galaxies, since the galaxies possess less gas to create stars, the NSCs have older population compared to late-type galaxies. However, we also find that NSCs are younger than their surrounding host galaxies. The physics isn't well understood and this is still an active field of research.

- **Kinematics:** The stars in NSCs usually rotate about the same direction as their host galaxies, no matter if they are in spirals or spheroidal galaxies. An useful quantity, $(v/\sigma)_{eff}$, is the ratio between the rotational velocity and velocity dispersion that tells us if the motion is influenced by rotation or random motion. In most of NSCs, the ratio is in the range of 0-0.5, while a few also exhibits a much higher ratio. (For the NSCs we will consider in our simulation, we will take this ratio as 2.)

3.2 Scaling Relations

Nucleation

It is important to ask whether NSCs appear in galaxies across the mass range. We define a term called "NSC occupation factor", which is the fraction of NSCs as a function of galaxy stellar mass. For early type galaxies, data shows that NSCs are present in $\geqslant 80\%$ in $10^9 M_\odot$ galaxies. The NSC occupation factor falls steadily as we go towards the low mass galaxies, reaching zero for galaxies of mass $10^6 M_\odot$. On the high end side, occupation factor similarly drops. A possible explanation is the disruption by SMBHs that are present in high mass galaxies. Another possible answer may be the existence a lot of BBHs. In the process of BBH formation and merger, they transfer a lot of energy to the surrounding stars as we saw in the last chapter. They may destroy the NSC too.

For late type galaxies, it becomes harder to distinguish the NSC but studies have been done (Georgiev and Böker [2014]). We find that for lower mass end, we have a small occupation number that peaks in the mass range of $10^9 - 10^{10} M_\odot$. What differs from the early type galaxies is the presence of NSCs in many high mass late type galaxies. Prime examples would be our Milky Way and Andromeda that despite possessing high stellar masses also have NSCs in their core.

In figure 3.2, the results discussed above are displayed. This image is taken from Neumayer et al. [2020]. The red and blue lines are the fitting lines while the shaded area is uncertainties. We see that for late-type galaxies, we have large uncertainties because of data obscured by dust and galactic light.

Studies have also found that even the galaxy's environments impacts the occupation factor. Sánchez-Janssen et al. [2019] showed that galaxies in Coma cluster had a higher occupation number than in Virgo cluster. A related study of radial distribution of galaxies with NSCs in clusters found that nucleated galaxies were more concentrated towards the center of the cluster(Ferguson and Sandage [1989]). In other words, occupation factor decreased with density of surrounding galaxies. However, these studies are done only for low-mass early type galaxies. Most of the late-type galaxies are in field but still possess NSCs. Our Milky Way and Andromeda are prime examples of this. This suggests that environment shouldn't affect galaxies across the Hubble classification but only the early type galaxies.

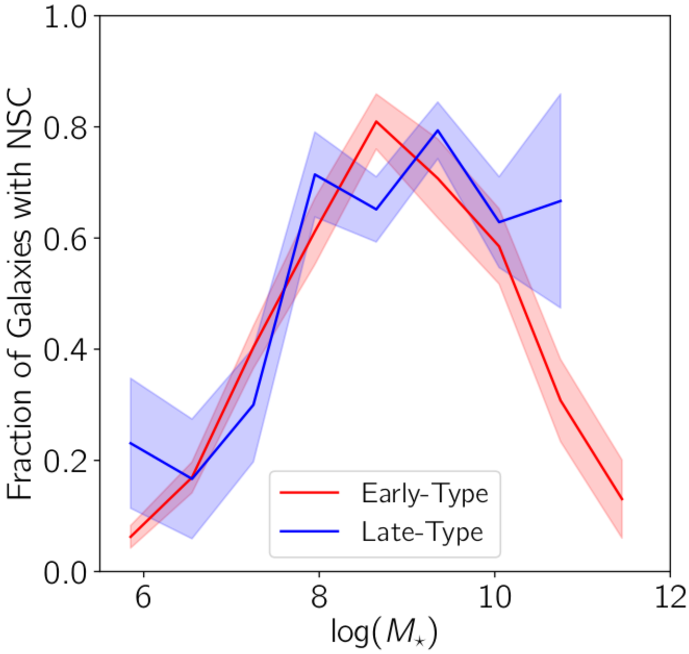

Figure 3.2: Fraction of NSC along the mass range of galaxies. For Early type galaxies, we see a sharp rise in NSC as mass increases to $10^9 M_\odot$ from where it steeply decreases. For Late type galaxies, we see a similar trend in the lower mass range. But we do not observe the decrease in NSC in heavier late type galaxies. Due to dust obscuring the light in late-type galaxies, we also have greater uncertainties, as shown in broader blue shaded area. Image credit:Neumayer et al. [2020]

Host type	c_1	c_2	α	β
NSC Mass-Galaxy Mass Relation $\log(M_{NSC}/c_1) = \alpha \times \log(M_{gal}/c_2) + \beta$				
Late	2.78×10^6	3.94×10^9	$1.001^{+0.054}_{-0.067}$	$0.016^{+0.023}_{-0.067}$
Early	2.24×10^6	1.75×10^9	$1.363^{+0.129}_{-0.071}$	$0.010^{+0.047}_{-0.060}$
Effective Radius-Galaxy Mass Relation $\log(r_{eff}/c_1) = \alpha \times \log(M_{gal}/c_2) + \beta$				
Late	3.44	5.61×10^9	$0.356^{+0.056}_{-0.057}$	$-0.012^{+0.026}_{-0.024}$
Early	6.11	2.09×10^9	$0.326^{+0.055}_{-0.051}$	$-0.011^{+0.015}_{-0.040}$
Effective Radius-NSC Mass Relation $\log(r_{eff}/c_1) = \alpha \times \log(M_{NSC}/c_2) + \beta$				
Late	3.31	3.60×10^6	$0.321^{+0.047}_{-0.038}$	$-0.011^{+0.014}_{-0.031}$
Early	6.27	1.95×10^6	$0.347^{+0.024}_{-0.024}$	$-0.024^{+0.022}_{-0.021}$

Table 3.1: Scaling relations between mass of the NSC, mass of the galaxy, and effective radius of the NSC taken from Georgiev et al. [2016]

.

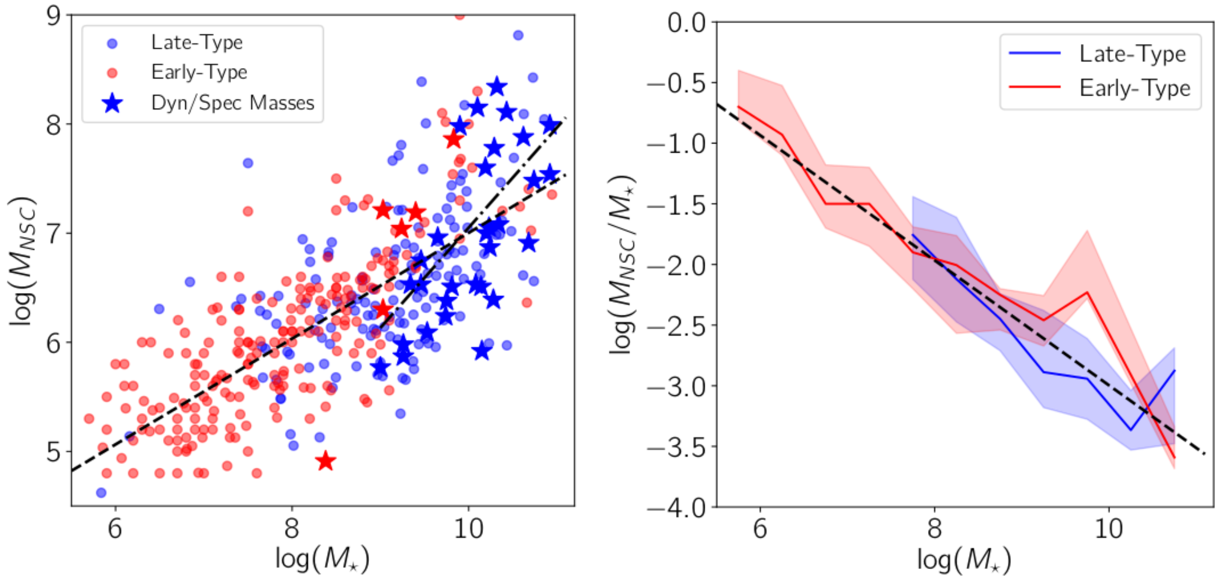

Figure 3.3: Left: Mass of NSCs versus mass of their host galaxies. For both early type and late type, we see an increase in NSC mass as the host galaxy mass increases. The black line in fitted to find a scaling relations between the two quantities. Late type galaxies show a much steeper trend than early type galaxies. Right: Mass fraction of NSC to their host galaxy as a function of host galaxy mass. For larger galaxies, their NSC constitute smaller percentage of their total mass. Image Credit: Neumayer et al. [2020]

3.3 Formation Channels of NSC

An important question is to ask: when did the NSC form? Was it before, together or after the formation of their hosts. As they lie in the central part of a galaxy where gas density is the highest, they may have been the earliest components of a galaxy. If this were true, the stars formed from this gas must be metal poor, so the seed population of stellar bodies in NSC must have low metallicity. In principle, this isn't easy to see. We have only been able to confirm this in nearby NSCs (Alfaro-Cuello et al. [2019]). For farther galaxies, we may be able to confirm if the NSC has a dominant older population of stars. However, as we already know from the above section, NSC host stars across the metallicities like our own Milky Way's NSC, prompting us to think of NSC's further evolution.

Globular Cluster Migration

In 1975, Tremaine et al. [1975] gave us the first scenario for the formation of M31 NSC. They proposed that GCs in the galaxy would be dragged to the galaxy's potential well through dynamical friction. (Similar to what we discussed in Chapter 2) This force would be linearly dependent on the GC's mass and inversely on velocity of the stars in the host galaxies. These GCs would form compact NSCs like the one we observe in M31.

This scenario was boosted by the deficit of GCs in the inner parts of early type galaxies. Another fact supporting this theory is the luminosity/mass ratio that is similar for both GCs and NSCs. This fact is something in-situ formation model cannot explain. How did NSC and GCs both have similar population when they are forming through different mechanisms. As discussed in the above section, the low metallicity population may also originate from this scenario. If a NSC is more metal poor than its surrounding, it is likely due to dynamically-driven formation.

N-body simulations performed to study this phenomenon tell us that GCs with mass above $10^5 M_\odot$ can indeed spiral into the galaxy's center within Hubble time. These simulations are also able to explain the sizes and density profile of the NSC. However, the existence of younger generation stars along with kinematics of NSCs suggest that a fraction of the NSC's mass was brought in by gas.

In-situ Star Formation

The younger star population was not something the globular cluster migration theory could explain. So, the theory of in-situ star formation was proposed. When gas reaches the center, an intense star burst can be triggered. If this process is repeated over the evolution time of a NSC, we can explain the composite stellar population we find. Supernova in the NSC and stellar winds may halt the infall of gas, until the cycle repeats. It has been shown that this cycle repeats on timescales of a hundred million years (Loose et al. [1982]). One can also argue that instead of gas, young stars spiral in to the center. Or YMCs have accreted instead of Gcs. However, if these two approaches were true, we should find young population on the outer rims of the NSC, which we do not. Moreover, observations show that these younger stars are flattened and rotating, which is to be expected if they formed from gas.

The in-situ star formation channel raised an important question. How is this gas transported to the central few parsecs of the galaxy? Mergers of gas-rich galaxies could be an answer as increase the gas concentration in the central region of the remnant galaxy. This could explain the NSCs of early-type galaxies but we find young population in even Late-type galaxies that haven't experienced such interactions. There are other mechanisms that bring gas, one of which is bar driven gas infall: Stellar bars in galaxies produce a non-axisymmetric potential that could bring that the gas inwards. This has been observed in spiral galaxy NGC6946 (Schinnerer et al. [2007]). Other possible answers may be magneto-rotational instability, tidal compression, and dissipative nucleation. Overall, it is possible to bring gas to the center of galaxies on timescales shorter than Hubble time and form NSCs.

Observations also tells us that the host galaxy may decide which of the two formation channel the NSC will take. Galaxies lighter than $10^9 M_\odot$ seems to prefer globular cluster migration while those above prefer gas infall. This is not a certainty but probability. Overall, there is evidence in support for both theories. We will need more observational data and more computationally expensive simulations to understand the process in much detail. Luckily, we are advancing on both frontiers.

3.4 Dynamics of NSC

Let us combine what we learned in this chapter with what we know from the previous chapter. The stellar bodies inside the NSC are all influenced by each other, gradually inspiraling towards the core. Dynamical friction acts on all bodies, the heavier one reaches the core faster. If this process was rampant, we would have an overly dense core that will eventually cause a runaway collision of stellar bodies. Fortunately, the dynamical processes in the core are intense, the stellar bodies can have their trajectories completely changed. As we saw in chapter 2, a lot of bodies are either completely ejected from the cluster or are just thrown towards the edges from three-body interactions. This relaxes the core and reshuffles the velocities and distribution of stellar bodies in the cluster. These two processes shape the cluster and its future.

3.5 NSC with SMBH

Most of the galaxies in the mass range $10^8 - 10^{10} M_\odot$ host an NSC. Above this mass range, the appearance of SMBH increases at the center of massive galaxies. A number of galaxies, our Milky Way included, have found NSC and SMBH existing with each other. In our Milky Way, a SMBH with mass $\approx 4 \times 10^6 M_\odot$ resides in an NSC of mass $\approx 3 \times 10^7 M_\odot$. Their coexistence is mostly found in galaxies with mass $10^9 - 10^{10} M_\odot$ above which, the NSC are destroyed.

Since this trend is very systematic and adding the tight scaling relations NSCs and SMBHs have with their host galaxies, these two separate components are indeed interrelated. The formation of SMBH, like NSC, is not very well understood. There are several formation channels out of which, we will focus on a single one, particularly, the formation of SMBH through runaway mergers of BHs in NSCs. The formation of intermediate mass black hole (IMBH) in NSC has already been shown by many studies (Mapelli et al. [2021]). They have also shown that NSCs are capable of producing IMBH with masses greater than $10^4 M_\odot$. The subsequent growth of massive black holes (MBHs) can be through various channels. The in-fall of gas that create bursts of star formation may also feed these MBHs. At the end of our thesis, we will also try to provide the answer to this question using the results we found.

3.6 NSC Model

For our discussion and future integration with FASTCLUSTER code, we will create a analytical model for NSC's growth. We will follow the analysis done by Arca-Sedda and Capuzzo-Dolcetta [2014]. They have shown that at center of galaxies, dynamical friction given by Chandrasekhar [1943] fails to correctly estimate the drag felt. Thus, with the help of N-body simulations, they formed a new analytical equation to explain dynamical friction time. We will use their equation along with an estimate of GCs to develop an evolutionary model for the NSC.

The distribution of GCs along the radial profile of the galaxy can be written as,

$$N_{GC}(r) = N_{GC,t} \left(\frac{r_{GC}}{r_{GC} + R_g} \right)^{3-\gamma} \tag{3.1}$$

where, $N_{GC,t}$ is the total number of GCs within a galaxy considering average GC mass and what fraction of galaxy mass does the GCs take and γ is the density slope for the galaxy. We will assume that one percent of the galaxy's mass is in globular cluster, then the number of clusters is, $N_{GC,t} = 0.01 M_g / M_{GC}$. R_g is the scale length of the galaxy, which is the radius where the galaxy's luminosity falls by a factor of e. Throughout the discussion of the thesis, whenever we mention accreting globular clusters, we only consider GCs within the scale length. The reason being that these GCs always have dynamical friction time lower than that of Hubble time. For lighter galaxies, we may be able to go way beyond the scale length, however, this consideration will give us a starting point upon which, we can build in the future. The relation between the scale length and mass of a galaxy is,

$$\left(\frac{R_g}{kpc} \right) = 2.37 (2^{1/(3-\gamma)} - 1) \left(\frac{M_g}{10^{11} M_\odot} \right)^k, \tag{3.2}$$

where $k = 0.14$ derived from the same paper. The new analytical equation developed by

Arca-Sedda and Capuzzo-Dolcetta [2014] is,

$$\tau_{DF} = \tau_0 g(e_{GC,\gamma})\sqrt{\frac{R_g^3}{M_g}}\left(\frac{M_{GC}}{M_g}\right)^{\alpha}\left(\frac{r_{GC}}{R_g}\right)^{\beta} \tag{3.3}$$

Here, τ_0 is a normalization constant and $g(e_{GC,\gamma})$ is a weak function of GC eccentricity and density slope of the galaxy. α and β are parameters of the infall that have been fitted through N-body simulations. Their values come out to be -0.67 and 1.76 respectively. Along with the density slope $\gamma = 1.8$, these values will remain constant for the course of the thesis. The infall rate is the number of GCs falling per unit time can be written as,

$$\dot{N}_{GC} = N_{GC}/\tau_{DF} \tag{3.4}$$

Combining equation equation (3.4) with equation (3.1),(3.2), and (3.3), we get the infall rate as,

$$\begin{aligned}\dot{N}_{GC}(R_g) =& 0.001Myr^{-1}\frac{1}{0.3\times g_{fact}\times(2.37(2^{1/(3-\gamma)}-1))^{3/2}}\left(\frac{r_{GC}}{r_{GC}+R_g}\right)^{3-\gamma}\\ &\times\left(\frac{M_g}{10^{11}M_\odot}\right)^{3/2(1-k)+\alpha}\left(\frac{M_{GC}}{10^{11}M_\odot}\right)^{-1-\alpha}\left(\frac{r_{GC}}{R_g}\right)^{-\beta},\end{aligned} \tag{3.5}$$

where,

$$g_{fact} = (2-\gamma)\left[\left(2.63\left(\frac{1}{2-\gamma}\right)^{2.26}+0.9\right)(1-e)+e\right] \tag{3.6}$$

The above expression can be understood better if divided into smaller terms. The most straightforward would be the mass of the galaxy and GC, the heavier they are, the faster the rate of accretion is. There is weak dependence on eccentricity, we have seen something similar in Chapter 2 for BBH case. Finally, there is a term for the density profile of the galaxy, which tell us how the GCs are spaced in the galaxy. There is also inclusion of the fact that the farther the GC is, the more time it will take to fall in. If we take inverse of equation (3.5), we arrive at 'Replenishment Time', which is the time between two successive GC infall events. Along with the dynamical infall timescales, they give us two important timescales to estimate our model.

$$t_{rep}(R_g) = (\dot{N}_{GC}(R_g))^{-1}. \tag{3.7}$$

Translating the infall rate to mass and adding to the initial mass of NSC, we can finally arrive at our desired expression. In the GC migration model, we assume that there is only gas at the center of the galaxy. The initial mass of the NSC is the gas encompassed in the central 10 pc of the galaxy, which will be our initial NSC size. Since, we are using Dehnen density profile, the initial mass can be calculated from this radius,

$$M_{init} = \left(M_g\frac{10}{10+R_g}\right)^{3-\gamma} \tag{3.8}$$

With this, we can write the mass of NSC at a given time, t, as

$$M_{NSC} = M_{init} + \dot{N}_{GC}\times M_{GC}\times t. \tag{3.9}$$

There are a few caveats that concerns validation of the above assessment but we will take the equation 3.9 as it is for now. Now that we have ab analytical equation to model the growth of a NSC, let us compare it with observational data to confirm our analysis. For simplicity, in

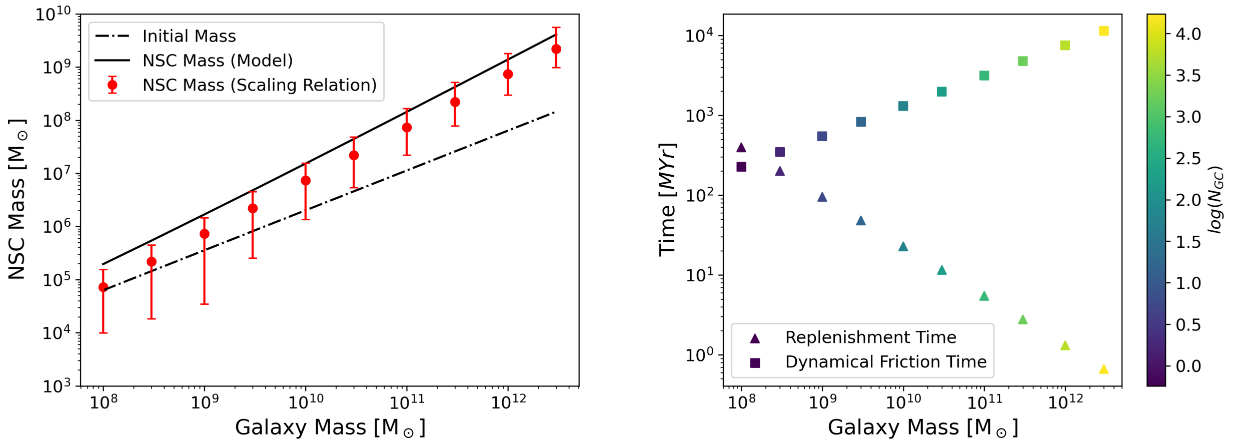

Figure 3.4: Left: Initial mass (dotted) and final mass (hard black) given by the model we just described above. The red scattered points are obtained from scaling relations of Georgiev et al. [2016]. Right: Replenishment time and dynamical friction time for GCs against that of galaxy mass. The color scale indicates the number of GCs within each galaxy.

equation 3.5, we will take $r_{GC} = R_g$, $M_{GC} = 5 \times 10^5 M_\odot$, and vary galaxy mass across a range.

As we can see from the figure 3.4, our model traces the observations quite well. A noteworthy thing is the fact that our mass always stays above the observed mass. A possible answer to it is that our model does not include the scenario of tidal forces that disrupt the GCs, preventing them from accreting. As such, we would always have a larger mass, which is not a big concern for the analysis we want to perform. The right figure tells us about the timescales on which the NSC grows and when it stops growing. For the lighter galaxies, we have fewer GC, which take a few hundred to a few thousand million years to migrate. On the other hand, for the heaviest galaxies, we have a merger event every million years.

To implement this method into FASTCLUSTER, we need time variance of the NSC mass. Let us consider the dynamical friction timescale and its dependence on radius,

$$\tau_{DF} = \tau_0 g(e_{GC,\gamma}) \sqrt{\frac{R_g^3}{M_g}} \left(\frac{M_{GC}}{M_g}\right)^\alpha \left(\frac{r_{GC}}{R_g}\right)^\beta . \tag{3.10}$$

For $r_{GC} = R_g$, we get the maximum dynamical friction timescale

$$\tau_{DF}(R_g) = \tau_0 g(e_{GC,\gamma}) \sqrt{\frac{R_g^3}{M_g}} \left(\frac{M_{GC}}{M_g}\right)^\alpha , \tag{3.11}$$

which is just the initial term of equation (3.3). So, we can write

$$\tau_{DF} = \tau_{DF}(R_g) \left(\frac{r_{GC}}{R_g}\right)^\beta . \tag{3.12}$$

We can invert this equation to write,

$$r_{GC} = R_g \left(\frac{t}{\tau_{DF}(R_g)}\right)^{1/\beta} \tag{3.13}$$

The above equation tells which specific radius of GC has been conquered at the particular time.

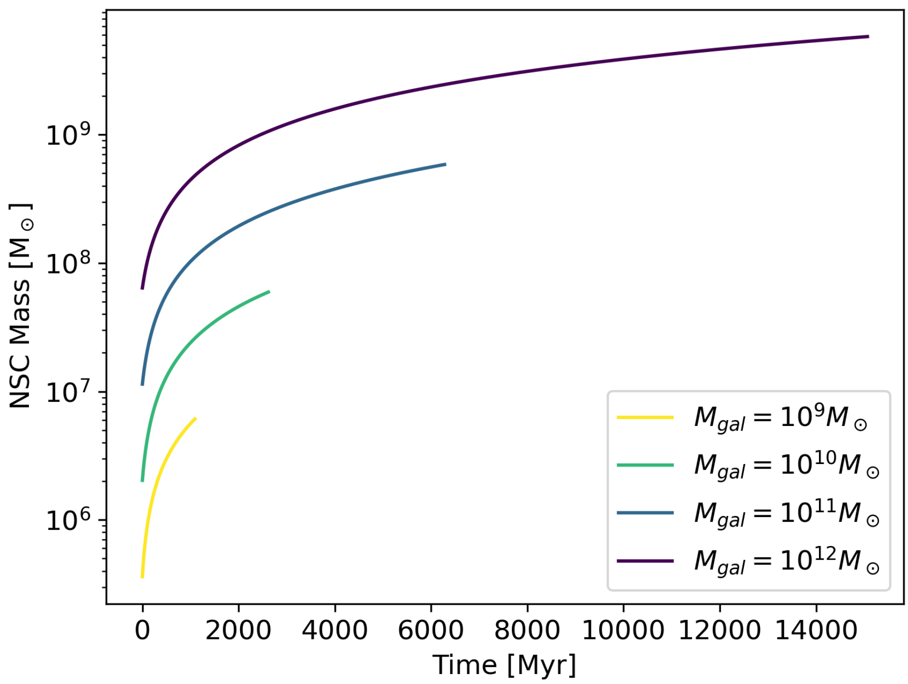

Figure 3.5: The mass evolution curves for NSC present in different galaxies masses according to the model described above. The accretion stops after the GC at scale length of the galaxy has accreted. This takes different times for different galaxies as shown in the figure. We also see that the mass of the NSC increases faster in the beginning that later, which can be attributed to the density profile of the galaxy.

Let's denote $\tau_{DF}(R_g)$ as T_R for simplicity. We can insert this into equation 3.5 to get,

$$\begin{aligned}\dot{N}_{GC}(R_g) =& 0.001 Myr^{-1} \frac{1}{0.3 \times g_{fact} \times (2.37(2^{1/(3-\gamma)} - 1))^{3/2}} \left(\frac{1}{1 + (T_R/t)^{1/\beta}} \right)^{3-\gamma} \\ & \times \left(\frac{M_g}{10^{11} M_\odot} \right)^{3/2(1-k)+\alpha} \left(\frac{M_{GC}}{10^{11} M_\odot} \right)^{-1-\alpha} \left(\frac{t}{T_R} \right)^{-1}\end{aligned} \tag{3.14}$$

where,

$$g_{fact} = (2-\gamma) \left[\left(2.63 \left(\frac{1}{2-\gamma} \right)^{2.26} + 0.9 \right) (1-e) + e \right] \tag{3.15}$$

Through a similar analytical calculation, we can define the infall rate at R_h, which is the half-mass radius. It is related to the rate defined above by,

$$\dot{N}_{GC}(R_h) = 2^{2-\gamma} (2^{1/(3-\gamma)} - 1)^\gamma \dot{N}_{GC}(R_g) \tag{3.16}$$

The other physical properties of the cluster can be derived from mass of the NSC (equation 3.9). The effective radius r_{eff} can be extracted using the scaling relations in table 3.1. Effective radius can be translated to half-mass radius through this equation,

$$r_{hm} = \frac{4}{3} r_{eff} \tag{3.17}$$

This equation is only valid for Dehnen density profile. The density and escape velocity of the cluster are defined as follows:

$$\rho = \frac{3M_{NSC}}{4\pi r_{hm}^3} \quad \text{and} \quad v_{esc} = \sqrt{\frac{2GM_{NSC}}{r_{hm}}} \tag{3.18}$$

In the table below, I have summarized the results of our model. All the results I displayed in table 3.2 and figure 3.4 were taken for late type galaxies. We can reproduce the similar results with early type galaxies too.

Galaxy Mass ($M_\odot$)	Initial NSC Mass ($M_\odot$)	Final NSC Mass ($M_\odot$)	Half-Mass Radius (pc)	Velocity (cm/s)	Scale Density ($M_\odot/pc^3$)
1.e+08	6.29e+04	1.95e+05	1.68	1.42+06	9.81e+03
3.e+08	1.44e+05	5.41e+05	2.33	2.00e+06	1.02e+04
1.e+09	3.56e+05	1.68e+06	3.35	2.94+06	1.06e+04
3.e+09	8.13e+05	4.78e+06	4.69	4.20e+06	1.10e+04
1.e+10	2.01e+06	1.52e+07	6.81	6.22+06	1.15e+04
3.e+10	4.59e+06	4.43e+07	9.59	8.94e+06	1.20e+04
1.e+11	1.13e+07	1.44e+07	14.0	1.33+07	1.25e+04
3.e+11	2.58e+07	4.23e+08	19.8	1.92e+07	1.30e+04
1.e+12	6.36e+07	1.39e+09	29.0	2.88+07	1.36e+04

Table 3.2: NSC properties for various galaxy masses.

Chapter 4

FASTCLUSTER

Gravitational wave astronomy take a different approach than light astronomy. We do not have a telescope pointed in a particular direction. Instead, we are detecting signals coming from all over the sky all at once. Adding this to the noise we have in detectors, an analogy would be looking at the sky, which is completely filled with sunlight. There is so much light that the light from stars and galaxy almost seems insignificant. To extract data from such noise, we can use a smart technique of convolution. If by any chance we know the waveform of a GW event, we can convolve this waveform to real time data, getting a spike if there is a signal hidden in all that noise. Still, we can only check if this one specific waveform is present in the signal, all the others would be missed. As we have seen in Appendix (A), the waveform depends on the orbital frequency and the masses of the binary. This is a simplified expression, the waveform has many other parameters that we haven't considered.

Thus, we should have a library of waveforms along with the physics behind each merger. N-body simulations can provide us with precise results to each merger, but it takes too long to explore the parameter space. It is even more impossible to simulate a whole star clusters with millions of stellar bodies for a few hundred possible binary mergers. So, we turn to semi-analytic codes. They may be less precise but they help explore the parameter space efficiently. With the tools we developed in Chapter 2 (2.16,2.12,2.23), we can concisely write the effects of a whole cluster on a BH with a few analytical equations. Adding on what we discussed in chapter 2, we will build upon and create a code that will simulate BH mergers in star clusters. The results of FASTCLUSTER can help create mock data for GW observations. From now on, all star cluster reference would be for NSC unless specified otherwise.

4.1 Initial Conditions

Star Cluster

Before discussing BHs, we will understand the environment they live in. In the basic version of FASTCLUSTER, there is no evolution of star clusters, they remain static in all their properties throughout the BHs evolution. The mass and density of the cluster are sampled from log-normal distributions with root mean square at 6 and 5 respectively. The standard deviation σ is assumed to be 0.4. This gives us a mass spread of $10^5 - 10^7 M_\odot$ and density spread of $10^4 - 10^6 M_\odot/pc^3$ as shown in figure 4.1. For each cluster, we also assume core density $\rho_c = 20\rho$. We extract escape velocity from mass and density using the relationship from Georgiev et al.

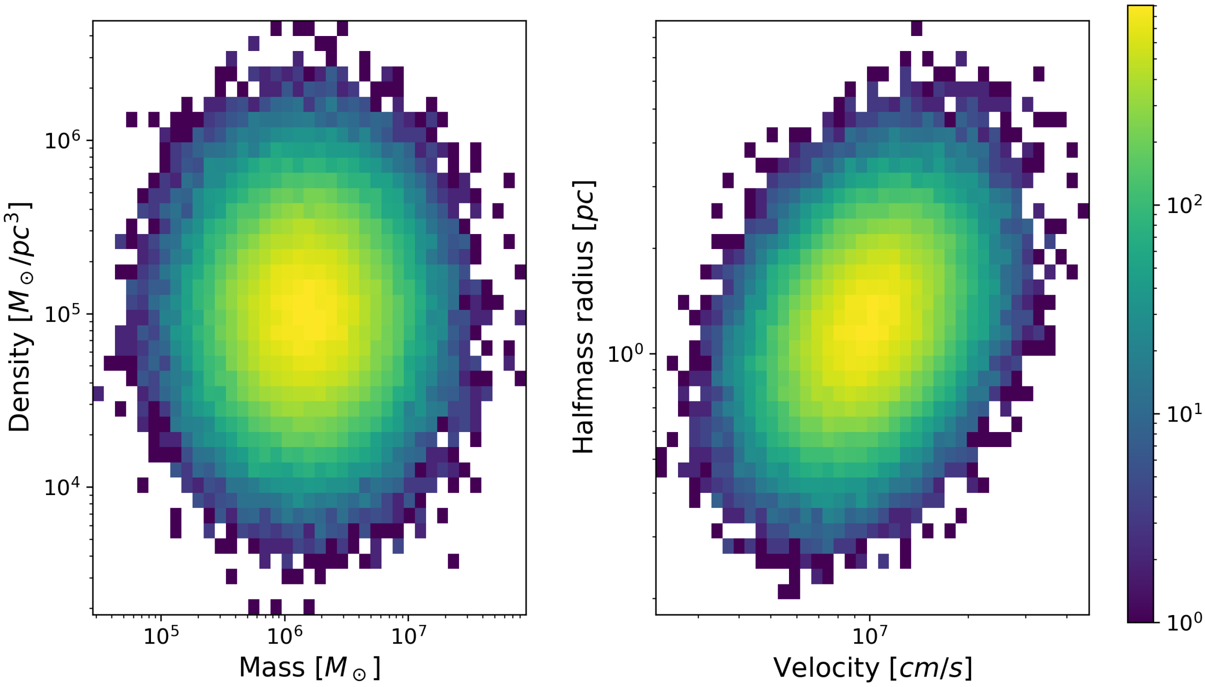

Figure 4.1: Left: 2D histogram of density and mass in an usual FASTCLUSTER run. Right: 2D histogram of half-mass radius and escape velocity. Density and mass are pulled from two radius normal functions so we get a 2d normal function aligned with the axis as their histogram. Half-mass radius and escape velocity are derived from them using equation 4.1 and 4.2

[2009],Fragione and Silk [2020],

$$v_{esc} = 40 \times 10^5 \left(\frac{M_{tot}}{10^5 M_\odot}\right)^{1/3} \left(\frac{\rho}{10^5 M_\odot/pc^3}\right)^{1/6}. \tag{4.1}$$

The half-mass radius is simply,

$$r_{hm} = \left(\frac{3M_{tot}}{8\pi\rho}\right)^{1/3} \tag{4.2}$$

The distribution of parameters in the clusters can be seen from the figure 4.1.

As we already saw in chapter 3, this does not cover the whole range of masses a NSC can have. We are not expanding to the whole parameter space for NSCs. However, that wasn't the goal of the basic FASTCLUSTER mode. It was meant to understand the difference brought by the median of different type of star clusters like GCs and YMCs. We will solve this when we introduce our model in the next chapter and see the changes it brings to the initial conditions too.

Black Holes

FASTCLUSTER is a population synthesis code, which mean we study a population of BHs having different parameters and see which BHs merge and why? The first step is to build a population of BHs that can be fed to FASTCLUSTER.

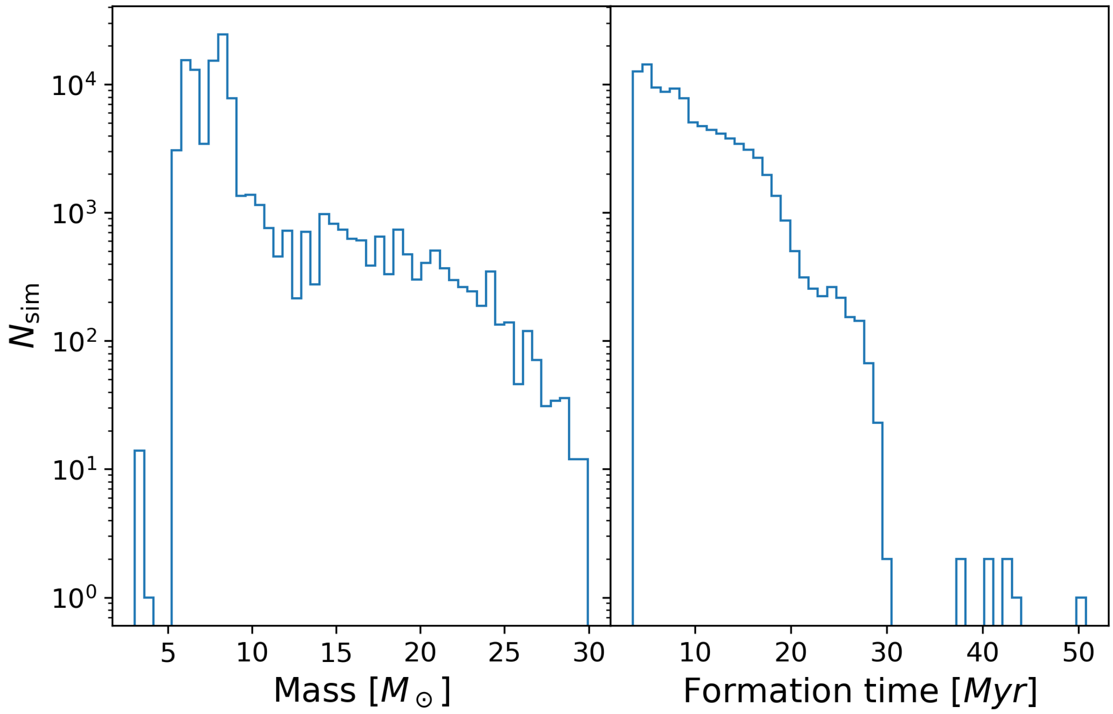

Figure 4.2: Left: Initial population of primary BH masses created using MOBSE. Since we are considering NSCs whose metallicity is high, we will constraint the mass range to $30M_{\odot}$. We see that this population is peaked at $7 - 8M_{\odot}$, which do not match the observation from LIGO-VIRGO. Right: The formation time of the BHs we have chosen. Most of them are formed within a few million years.

Masses and formation time: BHs are the end-points of massive stars. Depending upon the metallicity and initial mass of the star, we can create a library of BH mass through stellar evolution codes. We will use the catalogs developed through MOBSE (Giacobbo et al. [2018],Giacobbo and Mapelli [2018],Giacobbo and Mapelli [2019],Giacobbo and Mapelli [2020]). To create this catalog, we will use solar metallicity, z=0.02 since NSC are metal rich. This gives us an initial population that looks like figure 4.2.

The primary mass is taken randomly from the above explained library while the secondary mass is pulled from an interval $[m_{min}, m_1)$, where $m_{min} = 3M_{\odot}$ is the minimum mass a BH can have. This distribution takes into account that nth generation BH can form binary with another nth generation BH and also the fact the heavier BHs will prefer heavier partner. m_2 follows this probability distribution function,

$$p(m_2|m_1) \propto (m_1 + m_2)^4. \tag{4.3}$$

Spins Another important quantity that determines the end fate of merger remnants are the dimensionless spins (χ_1 and χ_2) of the BHs. We sample the spins from a Maxwellian distribution with mean of $\sigma_\chi = 0.1$, truncating the spins at $\chi = 1$. These parameters are inferred according to the data from GWTC-3.

Spins tilts: The direction of these spins (θ_1 and θ_2) are drawn isotropically over the sphere, from 0 to 2π

For each binary, we also calculate the effective spin (χ_{eff}) and precessing spin (χ_p) defined as,

$$\begin{aligned}\chi_{eff} &= \frac{(m_1\vec{\chi}_1 + m_2\vec{\chi}_2)}{(m_1 + m_2)} \cdot \frac{\vec{L}}{L} \\ \chi_p &= \frac{c}{B_1 G m_1^2} max(B_1 S_{1\perp}, B_2 S_{2\perp})\end{aligned} \tag{4.4}$$

Eccentricity and orbital separation: Eccentricities are drawn from a thermal distribution, $p(e) = 2e$ with $e \in [0, 1)$. The semi major axis is sampled from a distribution $p(a) \propto 1/a$ with $a_{min} = 1 R_\odot$ and $a_{max} = 10^3 R_\odot$. Along with this sampling, we check whether the binary is soft or not using the equation,

$$\frac{G m_1 m_2}{2a} \geqslant \frac{1}{2} m_* \sigma^2, \tag{4.5}$$

where m_* is the average mass in the cluster and σ is the velocity dispersion. This equation is a simple statement: if the binding energy of the binary is less than the average kinetic energy of stars, it will be easily destroyed by dynamical interactions. If the semi major axis sampled gives us a soft binary, we ignore it and call another sample. In such a way, all the binaries formed are hard binaries. Now, we have a physical system ready, we will simulate it as described in the next section.

4.2 Methodology

First Generation

After we have created a population of BHs, giving them mass and formation time, we try to find out which of these BHs can successfully form a binary through dynamical processes in Hubble time. We define a unique time t_{dyn},

$$t_{dyn} = max(t_{form}, t_{DF} + min(t_{3bb}, t_{121})), \tag{4.6}$$

where t_{form} is the formation time of the BH, t_{DF} is the time taken by the BH to migrate to the cluster's core through dynamical friction (equation 3.3), t_{3bb} is the time after which the BH will form binary through three body interactions (equation 2.12), and t_{121} is the time taken by BH to form a binary through exchanges (equation 2.16).

The assumptions went behind t_{dyn} are as follows. If the evolution time of a star is small, it would become a BH early on, way before dynamical friction could bring it to the core. In this case, the time it will take to form a hard binary is the time taken to bring it to the core and shape the binary through dynamical processes. Since three body interactions and exchanges are complimentary, we only need the process, which occurs faster. On the other hand, if the evolution time of the star is long. By the time it has turned to a BH, the star would already be in the cluster core in a hard binary.

Now, we check for the condition $t_{dyn} < t_H$, where t_H is Hubble time. We are only interested in mergers that could happen within Hubble time since we won't see them otherwise. For the BHs that satisfy this condition, we pair it up with a secondary BH, chosen according to equation 4.3.

Next, we check if the two BHs in the binary received supernova kicks strong enough for them to be ejected by the cluster. If they are ejected, we aren't interested since they will no longer contribute inside the cluster. The supernova kicks v_{SN0} are taken from a normal distribution with one dimensional root mean square at $265 Km/s$. We re-scale this kicks according to the mass of the BH by,

$$v_{SN} = v_{SN0} \frac{< m_{NS} >}{m_{BH}}, \tag{4.7}$$

where $< m_{NS} >$ is average neutron star mass, taken as $1.33 M_{\odot}$. If these two conditions are met, we assign these pair spins, orientations, orbital separation, and eccentricity. There is still a condition that can force the binaries to eject. It is the same process that tend to bring them together. In chapter 2, we discussed semi-major axis beneath which, a binary is ejected because of dynamical processes a_{ej} (eq 2.21) and simultaneously, we saw a distance at which, gravity becomes dominant. a_{GW} (eq. 2.34). Before starting the orbital evolution, we need to ascertain if $a_{GW} > a_{ej}$ or else the binary will be ejected.

The BHs that survive through these barrage of conditions can finally settle merge. The orbital evolution of the binaries is governed by equations 2.33 and 2.35. We follow Euler method to solve these two first order different equations,

$$\begin{aligned} a(t+h) &= a(t) + h f_a(t, a(t), e(t)) \\ e(t+h) &= e(t) + h f_e(t, a(t), e(t)) \end{aligned} \tag{4.8}$$

where $f_a(t, a(t), e(t))$ and $f_e(t, a(t), e(t))$ is the right hand side of equations 2.33 and 2.35 respectively. h is the time step of integration, which we adaptively change with each step. At each step, we also check if for the condition of $t + h < t_H$ since we want to avoid these kind of binaries. The evolution stops when semi-major axis, a, becomes equivalent to Schwarzschild radius of the BHs ($a \sim 2GM/c^2$).

At the end of this evolution, we get the final eccentricity, final orbital separation, and coalescence time of the pairs. We then calculate the remnant BH merger mass and spin according to fitting formulas from numerical relativity, as described by, Jiménez-Forteza et al. [2017]. The final mass is 0.9 of the total mass of merging BHs and the spins peak around 0.7-0.9. The remnant will also receive a relativistic kicks, modeled according to Lousto et al. [2012].

$$v_{kick} = \left(v_m^2 + v_\perp^2 + 2 v_m v_\perp \cos\phi + v_{||}^2\right)^{1/2} \tag{4.9}$$

where,

$$\begin{aligned} v_m &= A\eta^2 \frac{(1-q)}{(1+q)}(1+B\eta) \\ v_\perp &= H\frac{\eta^2}{(1+q)}|\chi_{1||} - \chi_{2||}| \\ v_{||} &= \frac{15\eta^2}{(1+q)}\left[V_{1,1} + V_A S_{||} + V_B S_{||}^2 + V_C S_{||}^3\right]|\chi_{1\perp} - q\chi_{2\perp}\cos(\phi_\Delta - \phi)| \end{aligned} \tag{4.10}$$

In the above equations, $q = m_2/m_1$ with $m_2 <= m_1$. $\eta = q(1+q)^{-2}$, $A = 1.2 \times 10^4 Km/s$, $B = -0.93$, $H = 6.9 \times 10^3 km/s$, $(V_{1,1}, V_A, V_B, V_C) = (3678, 2481, 1792, 1506) km/s$ respectively. χ_1 and χ_2 are spins of the BHs, which are separated into parallel and perpendicular according to the binary's orbital momentum. $S_{||}$ is the component of vector $\vec{S} = 2(\vec{\chi}_1 + q^2\vec{\chi}_2)/(1+q^2)$. Finally, ϕ_Δ is the direction of the infall at merger and ϕ is the phase of the binary. Both of these quantities are randomly drawn. If $v_{kick} < v_{esc}$, the remnant can stay in the cluster and repeat the process.

Nth Generation

Even if the remnant BH is not ejected by relativistic kick, it is thrown to the edges of the cluster. It must sink back into the core to repeat the process through dynamical friction. We once again calculate the dynamical time,

$$t_{dyn} = t_{merg} + t_{DF} + min(t_{3bb}, t_{121}), \tag{4.11}$$

where t_{merg} is the time taken by the previous generation binary to form and merge. If this time is less than Hubble time, we assign this BH a secondary according to the same distribution. After checking for their supernova kicks, we assign the binary a new eccentricity, semi-major axis, orientations. As for spin, the primary takes the remnant spin while the secondary's spin is taken from a random sample.

The evolution follows the same numerical formulas as first generation. We repeat this process until all the BHs have been ejected by the cluster or their merger time is larger than Hubble time.

4.3 Results

We have simulated 10^5 BHs in NSC mode of FASTCLUSTER code. Since there is no evolution to the properties of NSC, the dynamics of a single BH largely depends on its mass.

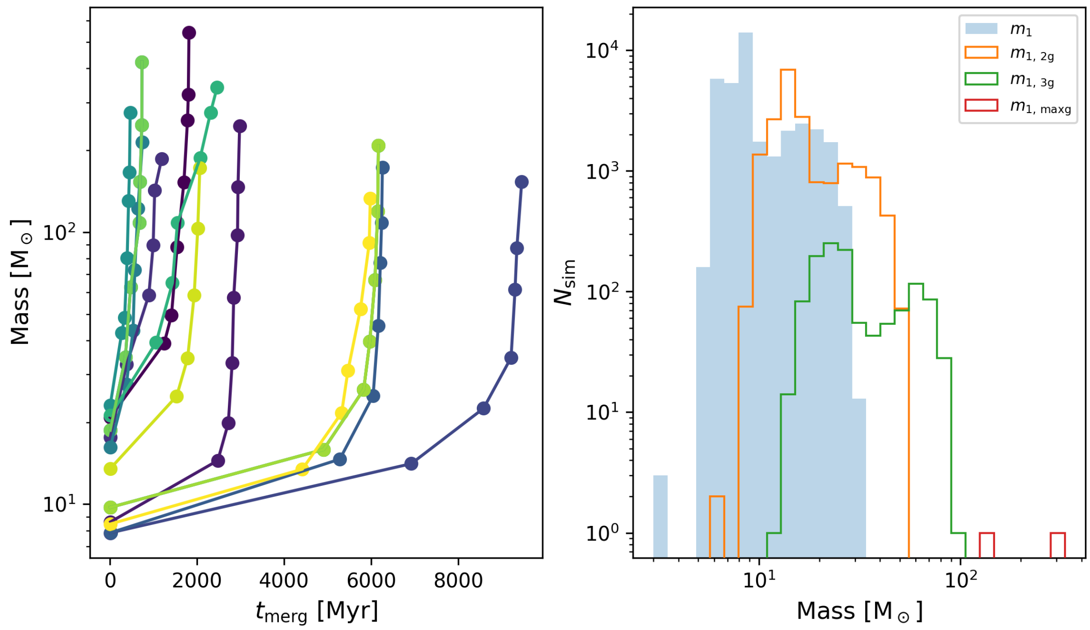

Figure 4.3: Left: BH growth chains. One particular line is the evolution track of one particularly BH. The first point is its formation and each following dot is a merger in its life. We see that in NSC, it is easy to have hierarchical mergers and form intermediate mass BHs. Right: The population of BHs that merge in the first, second, third, and seventh generation. With each progressing population, our population shifts right on the mass spectrum.

In the left plot of figure 4.3, we show the growth history of BHs through merger chains. Each line is the merger history of one particular BH. The first point is the mass and formation

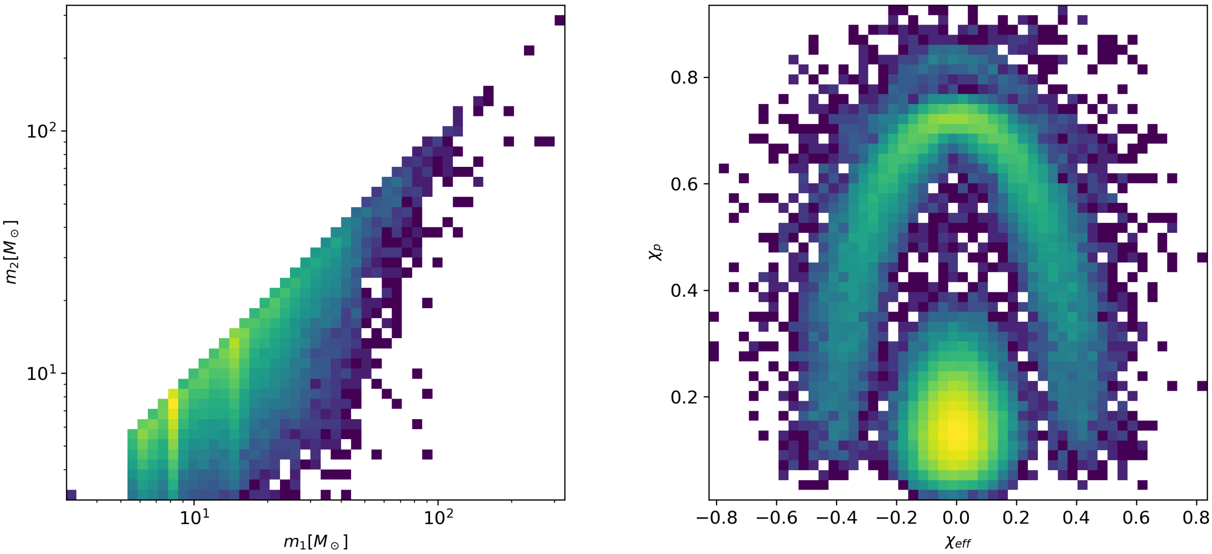

Figure 4.4: Left: Primary mass v/s secondary mass of the binaries that merge within our simulation. Right: χ_{eff} v/s χ_p histogram as shown in equation 4.4.

time of the BH while each progressing points represents a merger. The projection of the line connecting two points on x-axis is the addition of dynamical time and coalescence time and on y-axis is the increment of mass. We can see that the lines are heavily influenced by the mass of the BHs. The larger the mass, the smaller is the dynamical time (eq 4.6) for the binary's formation and merger. This causes a steep line between two points. Moreover, the higher the mass, the steeper the line becomes in most cases. This is easily seen for lighter BHs. They take longer to merger initially than speeding up as their mass increases. Mergers for which the line becomes almost vertical are called runaway mergers.

On the right side of figure 4.3, I have shown the populations of BHs of progressive generations. The two factors stopping BH from merging in our simulation is the BH being ejected from the cluster by supernova, relativistic kick or the BH taking too long to form a binary and merge. We will see these two forces shaping the dynamics of BHs for our work in chapter 6.

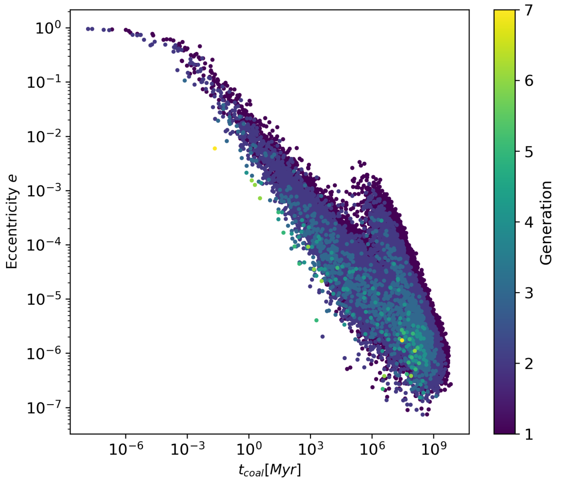

Figure 4.5: Final eccentricity v/s coalescence time of BH binaries. The color scheme is according to the generation of BHs. We see that FASTCLUSTER is able to produce highly eccentric mergers for whom, the coalescence time is very short. We also notice that with progressive generations, the coalescence time is also shortening since BHs are getting heavier.

Stellar dynamics in dense cluster systems can produce highly eccentric binaries, that lose energy more rapidly than binaries in circular orbits. More energy loss means shorter coalescence times: this can be observed in figure 4.5. The coalescence time also depends on the semi-major axis of the binary, since larger separation would imply a greater time (eq. 2.6).

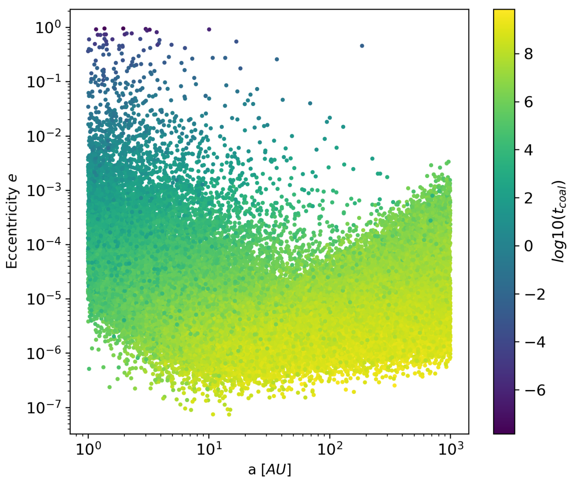

Figure 4.6: Eccentricity versus semi-major axis of the BH binaries that merger. The color scheme is according to the log of coalescence time of the binaries. Coalescence time decreases with shorter semi-major axis and higher eccentricity. The bit of noise in the color scheme is due to different BH masses.

Chapter 5

Black Hole Population Synthesis

The basic form of FASTCLUSTER does it job very well. We are able to explore the parameter space of clusters and BHs to find dynamical mergers. However, not all pairs of parameters create a realistic physical system. For example, a cluster of mass $10^6 M_\odot$ cannot have a density of $10^5 M_\odot/pc^3$ unless is size is around $1pc$, which is a little improbable. Moreover, realistic systems may hide under all the randomness we have created. If our goal is to simply study the mergers in realistic clusters, we may have to sacrifice some of the freedom in parameter space and turn to physical properties that depend on each other. An example would be the change in mass and density relation. Previously, these quantities were taken independent of each other but we know its not true. The more mass a cluster has, the more radius it would have (generally), so density would directly and indirectly depend on the mass of the cluster. We will make several such changes to the working of the population synthesis to achieve our goal.

5.1 Initial Conditions

Star Clusters

We will use the mathematical expressions developed in Section 3.6 to now define the initial parameters of the star cluster. For the initial mass of the cluster, we will use the mass enclosed within 10 pc of the galaxy's radius. This will add galaxy mass as an additional parameter in our code along with various other parameters such as the density profile and so on. We will also have additional parameters that are important to the evolution model like α and β but since we are keeping them constant throughout the work, we won't dive into them. To increase the parameter space by a little, we will also introduce a scatter that will change the initial mass adequately that we can explore some of the parameter space while consequently not drifting too far from a realistic system.

For the radius of the cluster, we will once again take help of Georgiev et al. [2016].

$$\log(r_{eff}/c_1) = \alpha \times \log(M_{NSC}/c_2) + \beta, \tag{5.1}$$

where c_1, c_2, α, and β are values taken from table 3.1 according to the parameter of galaxy type. In figure 5.1, the histogram are created with a random ensemble where galaxy mass can vary between 10^9 to $10^{12} M_\odot$ and galaxy type can vary between late and early. Density and escape velocity will be calculated through these simple formulas,

$$\rho = \frac{4}{3}\pi r^3, \tag{5.2}$$

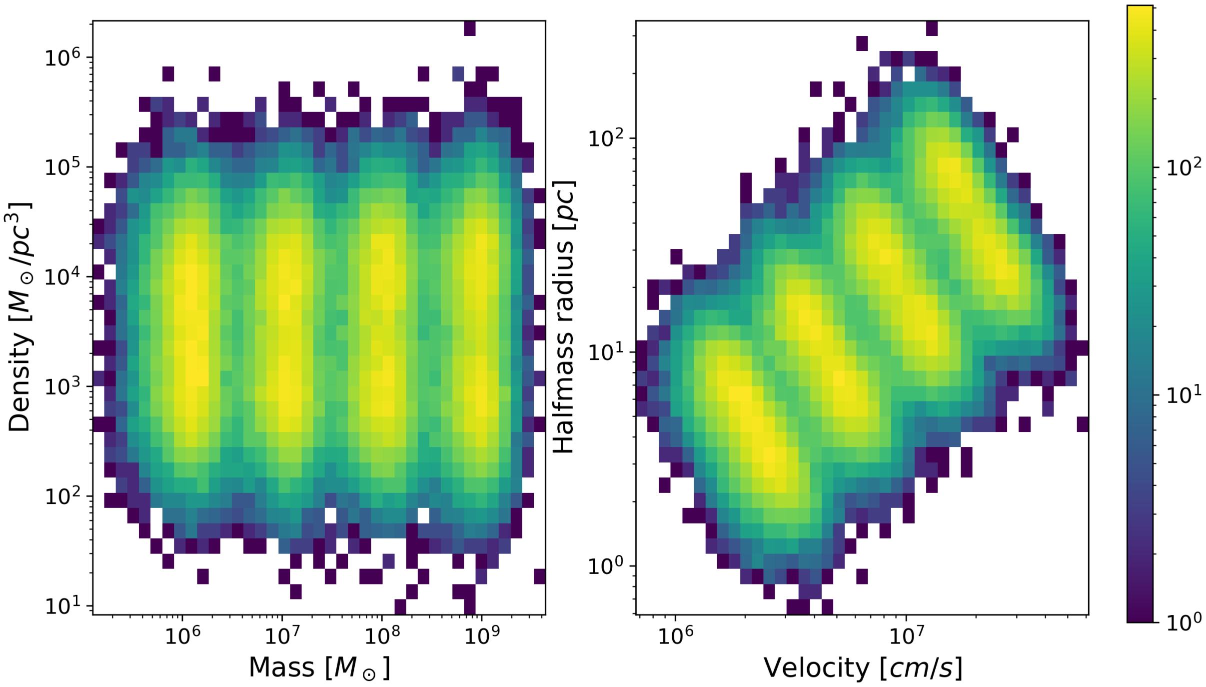

Figure 5.1: Left: Mass and Density of the clusters our BHs will live in. This is created from combination of all galaxies from 10^9 to $10^{12} M_\odot$ along with early and late type galaxies. The four peaks in both plots are for four different galaxy masses. We can see that for galaxy of one particular mass, we have a small parameter space. Conversely, as a whole, the parameter space is increased in all four quantities.

$$v_{esc} = \sqrt{\frac{0.4GM_{NSC}}{r_{hm}}} \tag{5.3}$$

Velocity dispersion is simply half the escape velocity as before. We get the following parameter spread.

Black Holes

As shown above, NSC possess gas before the GC migration starts. Stars can form from this gas, eventually evolving to BHs. The distribution of these BHs would be similar to stellar evolution codes that we have used before. However, this mass is just a small fraction of the total mass that would arrive later through globular clusters.

As shown in Mapelli et al. [2021], globular clusters also exhibit hierarchical mergers. Using FASTCLUSTER, we create a library of BHs in globular clusters. We want all the BHs that weren't ejected from the cluster, either by supernova or relativistic kicks. A large portion of these BHs would be the ones who had dynamical time greater than Hubble time, so they couldn't do anything other than just sitting inside the globular cluster. Naturally, to make our synthesis more realistic, we simply can't take all the BHs a globular cluster may have. We also have to took at when a globular cluster fell into the center and pull a BH according to it.

From figure 3.5, we see that according to our current model, the accretion stops when all the globular clusters within the scale length of the galaxy have spiraled in. Moreover, the accretion curve is not linear. More globular cluster accrete in the earlier years than later. The formation

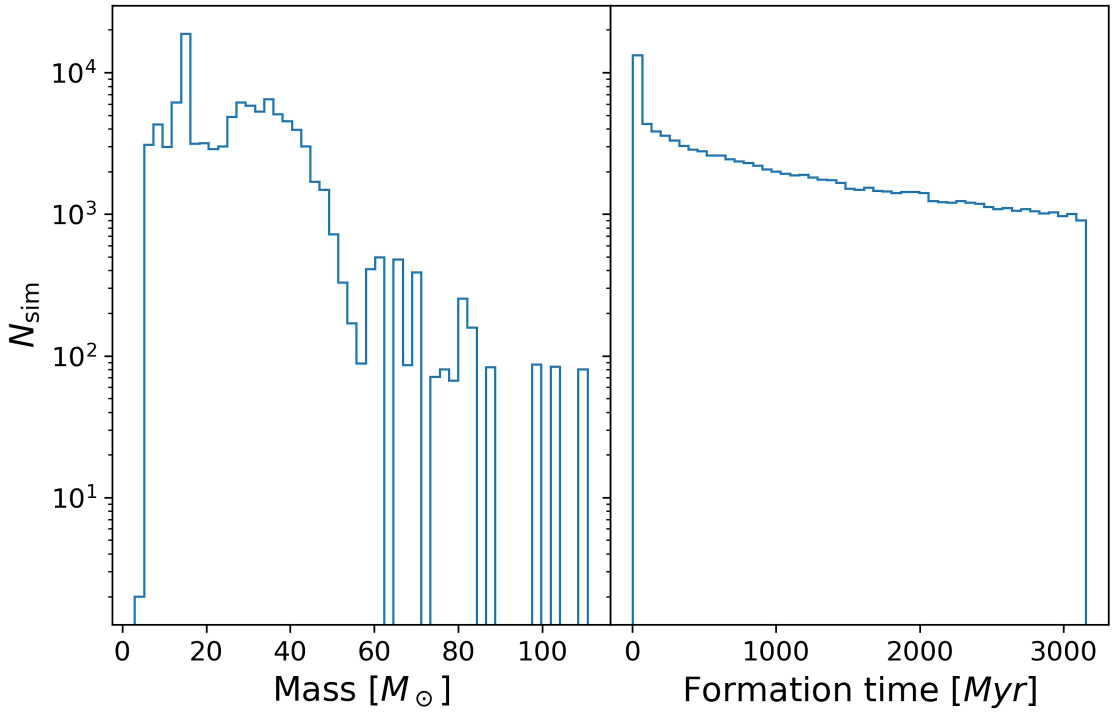

Figure 5.2: Left: Population of masses we get from BH from globular cluster. This includes the BH that have merged to create heavier BHs too. Right: This is no longer the formation time but the time these BH accreted onto the NSC. This particular population is for a NSC forming in a galaxy of mass $10^{11}M_\odot$ where accretion stops around $3000Myr$. The peak at lower times comes from the BHs that formed in the NSC, i,e, local BHs.

time of the migrating BHs follows a non-linear curve.

The remaining properties of BHs such as eccentricities, spins, and orientations are kept the same as the basic FASTCLUSTER.

5.2 Methodology

In the previous section, we only focused on BBH evolution, but this time, we would also evolve the NSC along with it. For each BH, we will calculate the dynamical time using equation 4.6. To calculate dynamical friction, three body and exchanges timescales, the inputs of NSC like velocity dispersion and density are taken at the instant the BH was formed. A different way of writing 4.6 is,

$$t_{dyn} = max(t_{form}, t_{DF}(t_{form}) + min(t_{3bb}(t_{form}), t_{121}(t_{form}))) \tag{5.4}$$

The density and velocity dispersion that enter the above equation are $\rho(t_{form})$ and $\sigma(t_{form})$. After checking that the dynamical time is less than Hubble time, we give the BH a companion according to distribution 4.3. Now that we also have a population of BHs also coming from globular clusters, we need to update how we check for their supernova kick. Internally, we know for each BH if it originated in the NSC or is migrating through a GC. We will call them "Local" and "Infall" BHs respectively. For local BHs, their is no difference, we take normal distribution with the root mean square at $265Km/s$ for their supernova kick and escape velocity at the formation time of the BH. (equation 4.7,5.3). The infall BHs can further be divided into two

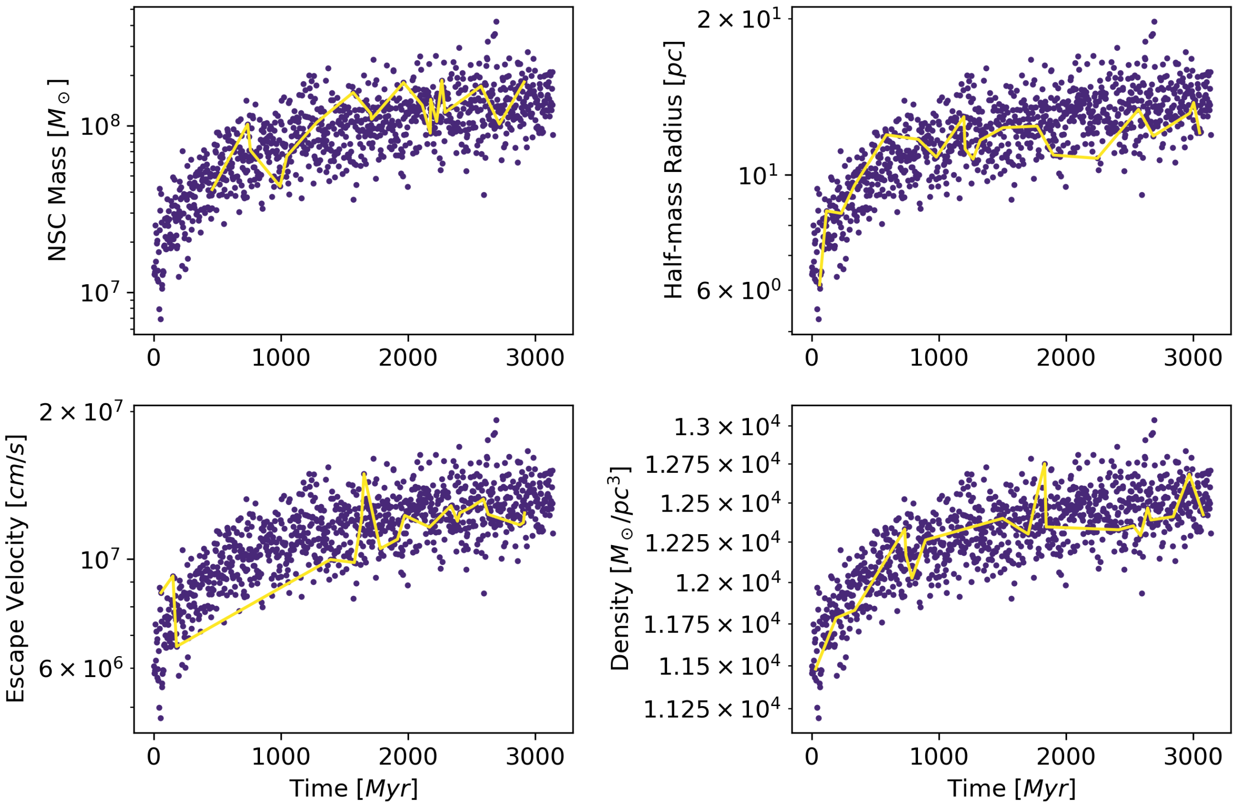

Figure 5.3: Evolution of NSC properties with time. With scatter implemented, the NSC does not follow a straight line but does a Brownian motion in the parameter space as shown by the yellow line

categories, first generation and nth generation. If they are first generation, their supernova kick is as the same as above but the escape velocity is considered according to the globular cluster. Considering the average mass of a globular cluster, we have set this escape velocity at $29.4Km/s$. Lastly, for the nth generation BHs, we consider their relativistic kicks instead of supernova kicks, which can also be found out through FASTCLUSTER. This conditions are set true for both companions.

Once the binary survives the kicks, we assign them spins, orientations, semi-major axis, and eccentricities in a similar way. We will calculate a_{ej} and a_{GW} and see that $a_{GW} > a_{ej}$, otherwise ignore that binary for all further cases.

The orbital evolution is similar, we numerically evolve the semi-major axis and eccentricity until the BH mergers. Note that in equation 2.33, 2.35, we have density and velocity dispersion of the NSC. These quantities will change with time throughout the orbital evolution.

Chapter 6

Results

6.1 Simulations

Using the methodology described in chapter 5, we have ran three simulations. We will simply call them Local BH, Late-type galaxy (LL), Local BH, Migratory BH, Lale-type galaxy (LML), Local BH, Migratory BH, Early-type galaxy (LME). In all three simulations, the NSC is evolving through the model described in Chapter 3 and 5. Their difference originate from the initial BH population we take. In LL runs, we consider BHs forming in the NSC throughout the GC accretion, i.e. we take mass population from stellar evolution in NSC as in chapter 4 and formation times (t_{form}) according to our discussion in chapter 5. We did this to understand the changes brought by a different mass distribution to dynamics of BBHs.

Simulation	Galaxy Mass $M_\odot$	Max m_{merg} $M_\odot$	N_g
LL	10^9	145.54	3
LL	10^{10}	192.40	4
LL	10^{11}	526.41	6
LL	10^{12}	119.92	3
LML	10^9	279.98	4
LML	10^{10}	652.61	6
LML	10^{11}	2360.41	10
LML	10^{12}	15900.13	12
LME	10^9	299.01	3
LME	10^{10}	388.31	4
LME	10^{11}	826.02	5
LME	10^{12}	735.72	4

Table 6.1: Maximum merger mass and generation of BHs produced in each simulation.

In LML and LME, we have taken the formation times and mass population as we would get from the globular clusters. The parameter we change is the type of galaxy. They are taken as late-type and early-type respectively. The major difference brought by this parameter is the radius of the NSC. In early-type galaxies, the clusters are much larger than late-type. Although this may not impact the escape velocity and mass of the clusters, it heavily alters the density of the cluster, therefore all the dynamical processes.

Each simulation is grouped together with four sub-simulations of four different galaxy masses

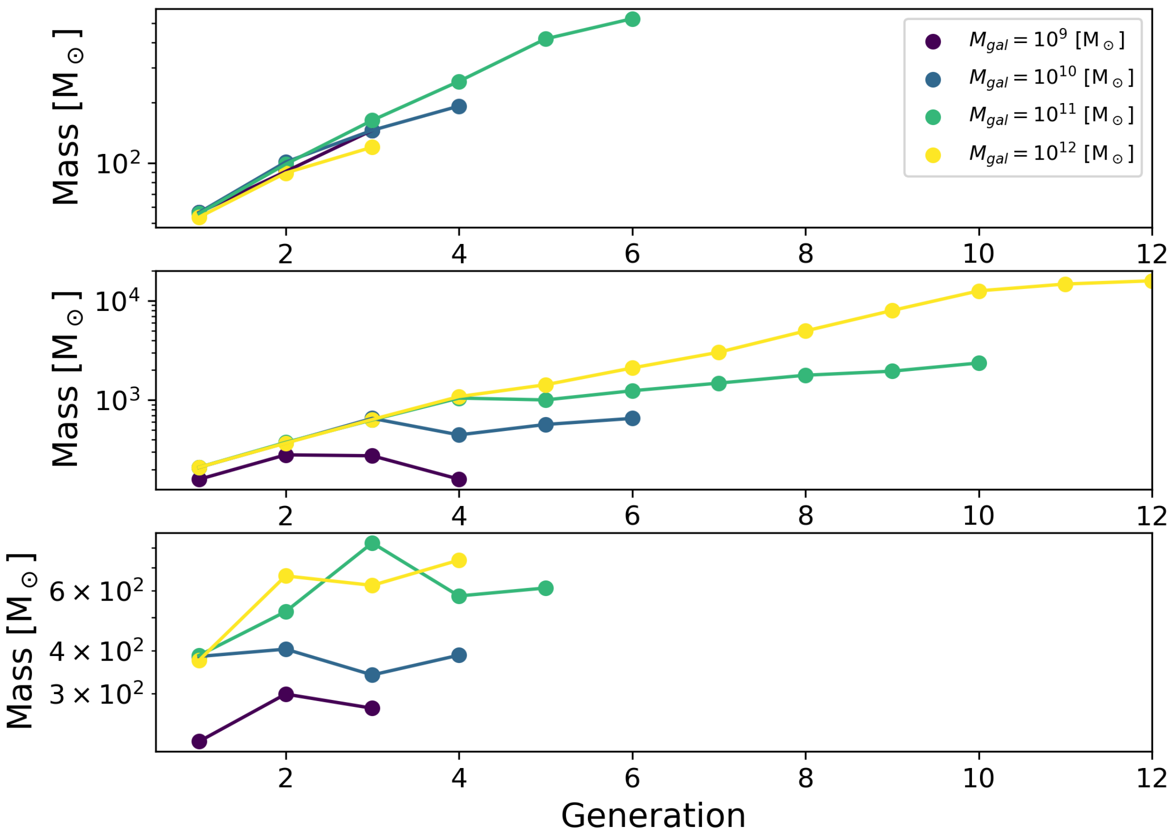

Figure 6.1: Maximum mass of primary BH that merge with each generation. From top to bottom: LL, LML and LME.

$(10^9, 10^{10}, 10^{11}, 10^{12} M_\odot)$. With scatter implemented, we are able to form NSCs for different masses and sizes. There are 10^5 BHs in each sub-simulation, which makes it easy to compare between the simulations.

In table 6.1, we can see the heaviest BH each simulation has produced along with the maximum generation they reached. Each NSC, from the lightest to heaviest is capable of producing IMBHs. A major change we observe is that with the addition of migratory BHs (heavier BH population), the efficiency of hierarchical mergers increases. In LL simulation, we are only reaching sixth generation while in LML, we go up to twelfth generation, producing BH greater than $10000 M_\odot$. We will discuss the reason for this change in the following sections. Lastly, in LME, the decrease in density have once again reduced the efficiency of hierarchical mergers.

Figure 6.1 is showing the maximum merger mass for each generation. Each color chain if for one particular galaxy. For coherence, we will use the same color scheme across the chapter unless specified otherwise.

6.2 Timescales

As we have seen in chapter 2 and chapter 5 (eq 2.24,2.12,2.16,5.4), the timescales are heavily dependent on the cluster properties like density and velocity dispersion along with BH masses.

Higher density decreases the timescales while higher velocity dispersion increases the timescales. This can be seen from the figure 6.2. In the figure, the four colors signify four galaxy masses while the three plots display the information of three major runs. Each point is the average time taken by a BH to form a hard binary according to equation 5.4 in that generation.

For galaxies of higher mass, the dynamical time is generally higher since NSCs are more massive and so is the velocity dispersion. A BH can form hard binary within a few million years in the lightest NSC, while it can take billions of years in the heaviest NSC. Another trend to notice is the decrease in dynamical time with increasing generation. It is straightforwards that each leading generation is later in time, which means the NSC has accreted more matter, become more massive, and have higher velocity dispersion. However, with progressing generation, the BH masses are also increasing. These two parameters have opposite effect on timescales with mass winning. It leads to shorter dynamical time as NSC evolves. This trend is only broken in the heaviest NSC in LL and LME. In these two cases, mass is unable to overcome the effect of velocity dispersion.

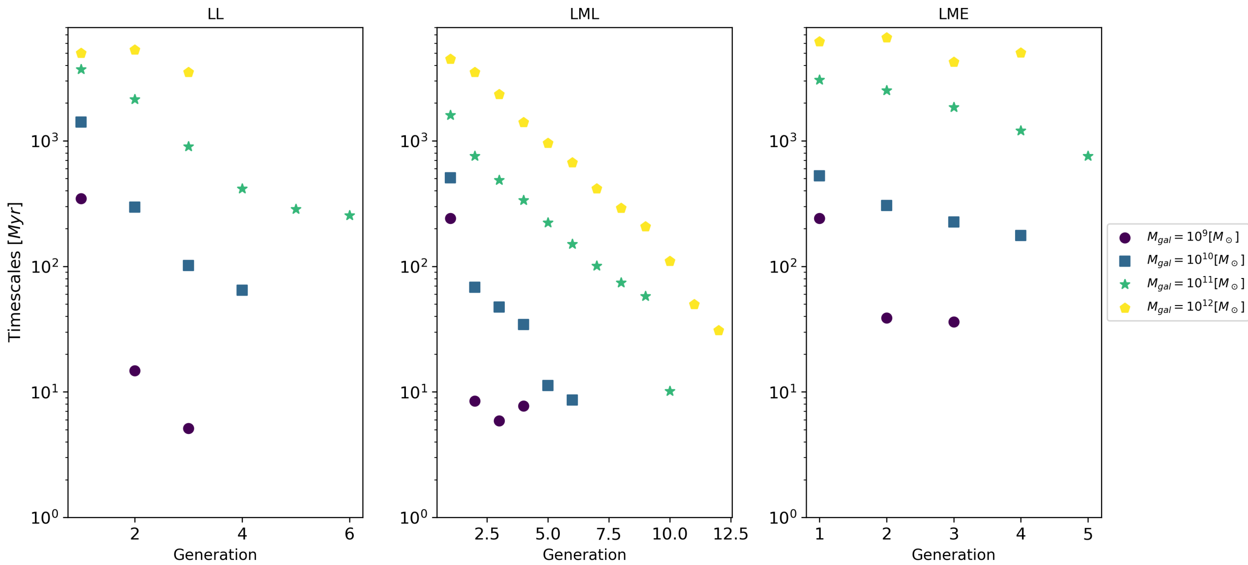

Figure 6.2: Dynamical timescales for all the 12 simulations. The three subplots are of three major runs while the different color markers are for different galaxies. The points shown here are the average for all the BHs within that generation.

6.3 Population

In the above section, we saw that heavier NSCs have long dynamical times, which implies the BHs can't have many hierarchical mergers. This is the key factor stopping mergers in heavier NSCs. On the other hand, lighter galaxies have small escape velocities, so supernova kicks and relativistic kicks are able to expel the BHs from the clusters. As for NSCs of intermediate mass, both forces act depending on the BH mass.

In $10^9 M_\odot$ run of LL simulation, we only have 933 BH mergers out of 10^5 initial BHs. The remaining 99% were thrown out of the cluster due to small escape velocities. Among the 933 that merged, a majority of remnant BHs were expelled by relativistic kicks with only 78 forming second generation BHs. Because of small dynamical time for lighter galaxies, all of these

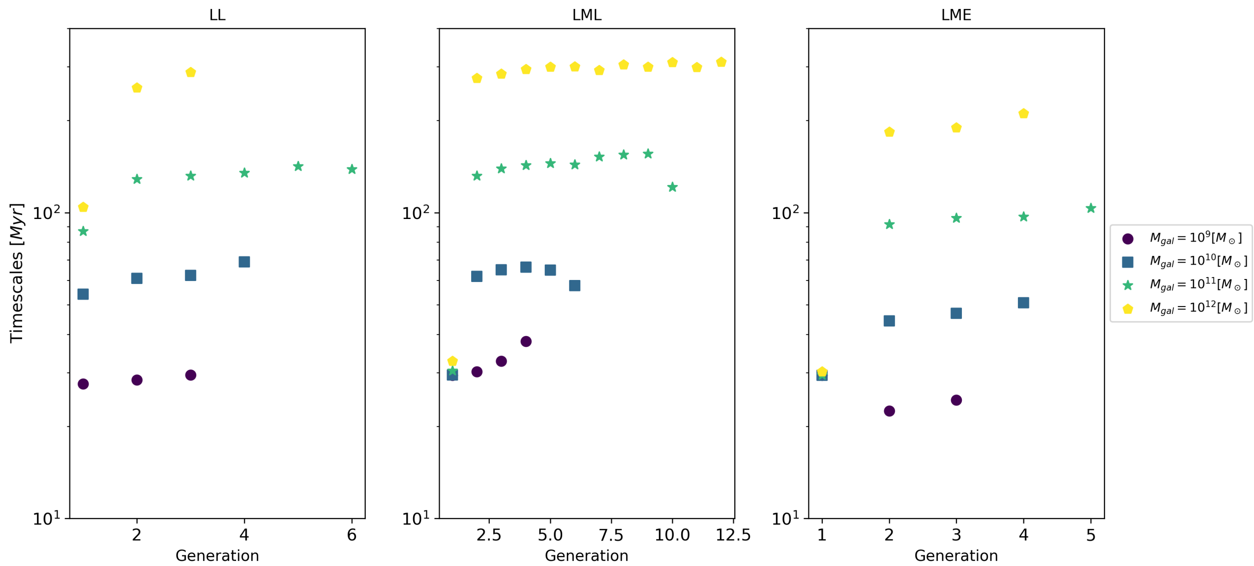

Figure 6.3: Mean escape velocities of all 12 simulations along the generations

BHs were able to merge within Hubble time. Most of the remnants were once again ejected from the cluster with only 2 BHs forming third generation. On further merger, these two were also ejected, causing the simulation to stop at third generation. Even though the NSCs was growing, they weren't able to retain the BHs.

On the other end of mass spectrum, for $10^{12}M_\odot$ run of LL simulation, most of the BHs remained in the cluster. However, due to longer dynamical time and coalescence time, only 738 BHs were able to merge within Hubble time. Because of the NSCs' heavier mass, none were ejected and only thrown to the outskirts of the clusters. Because of their long coalescence time, the NSCs have grown a lot, having greater velocity dispersion. Dynamical friction time for these BHs was too large So, only 43 become second generation. The simulation also stopped at third generation with only 5 BHs merging.

In the 10^{10} and $10^{11}M_\odot$ galaxy runs, we have a balance of ejection and longer times. These two mass ranges are the most efficient with the latter simulation producing the heaviest mass remnant of the LL simulation.

In the LML runs, we are also considering masses of BHs coming from globular clusters. The peak in mass shifted from $7 - 10M_\odot$ to two peaks at $12 - 15M_\odot$ and $30 - 35M_\odot$ with a long tail going more than a hundred $M_\odot$. In the lighter NSCs, the change in mass have altered the distribution of supernova kicks since they are inversely proportional to the BH mass (eq. 4.7). Additionally, we are considering the escape velocities from GCs for the BHs that are infalling. This creates a more realistic system. Their combined effect still produces a higher number of mergers in the $10^9M_\odot$ galaxy run with 43841 BHs merging in the first generation. The relativistic kicks are the same, they do not depend on the mass of the primary but rather the fraction $q = m_2/m_1$ (eq. 4.9). These kicks remain similar to LL runs, ejecting a lot of BHs from the lighter NSCs. The simulation stops at fourth generation.

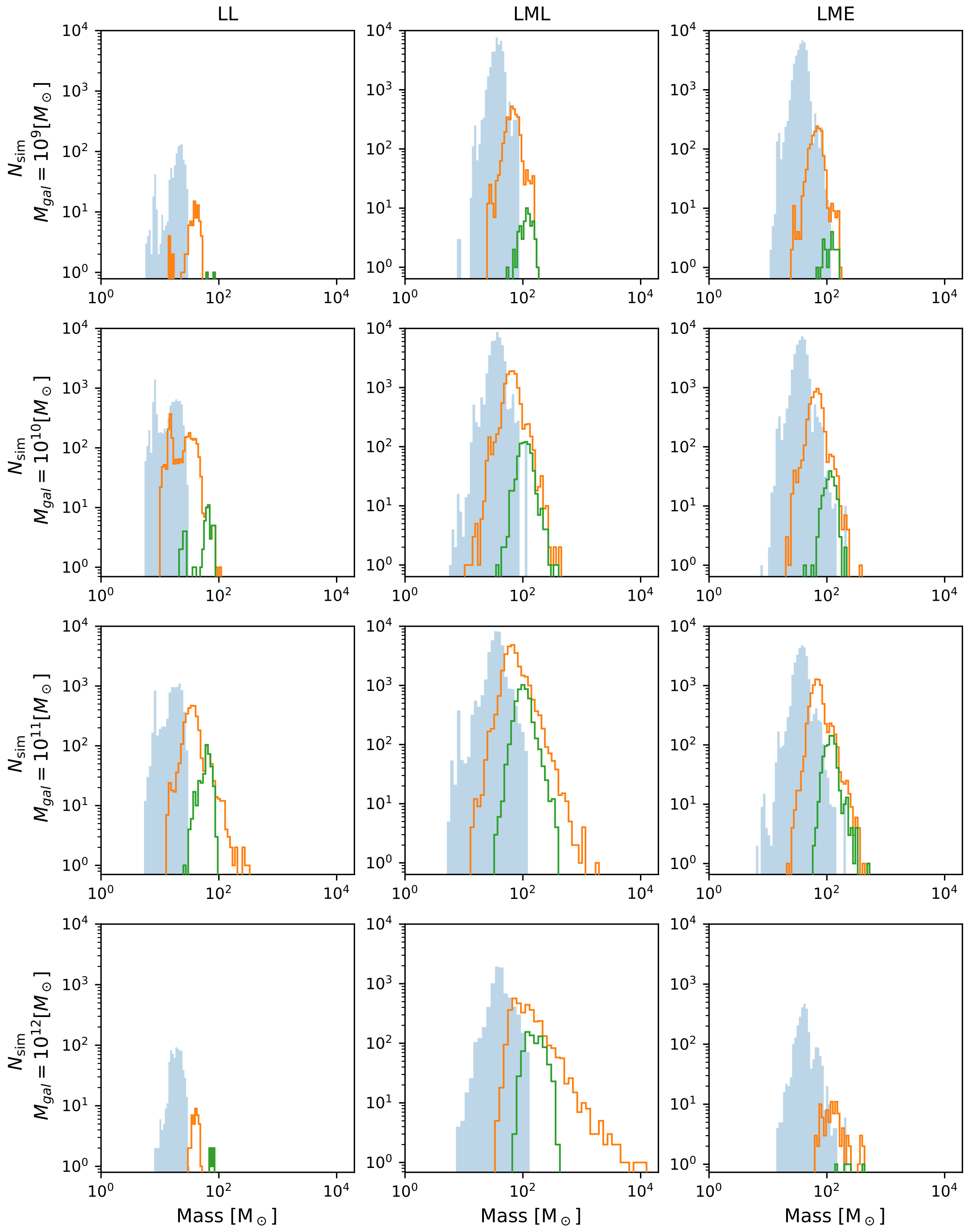

Figure 6.4: Population of BHs that merge with all 12 simulations. The blue filled population is first generation, orange is second generation and green is third generation. It is clearly shown that LML runs produced the most BH mergers.

For $10^{12} M_\odot$ run, we saw earlier that most of the BHs were retained in the NSCs. The increase in mass will effectively bring dynamical time of many of these BHs down, leading to many first generation mergers, 7902 exactly. With greater mass, the coalescence time is also small, so the NSC has not grown a lot within that time. The effect caused by increase in mass overcomes the effect caused by increase in velocity dispersion. We have a greater amount of BHs going to higher generations.

The runs with galaxy mass 10^{10} and $10^{11} M_\odot$ have similarly many BHs surviving and reaching higher generations.

Lastly, in the LME runs, we see the effect of density on the dynamics of BHs. Changing the galaxy type from late to early, we decreased the average density from $11000 - 13000 M_\odot/pc^3$ to just $700 - 800 M_\odot/pc^3$. The efficiency brought my increasing BH mass is canceled by the sparser NSCs. Although a lot of BHs survive ejection from BH, we do not get higher generation BHs. From table 6.1, we see that we only go maximum fifth generation in all LME runs.

6.4 BH Growth History

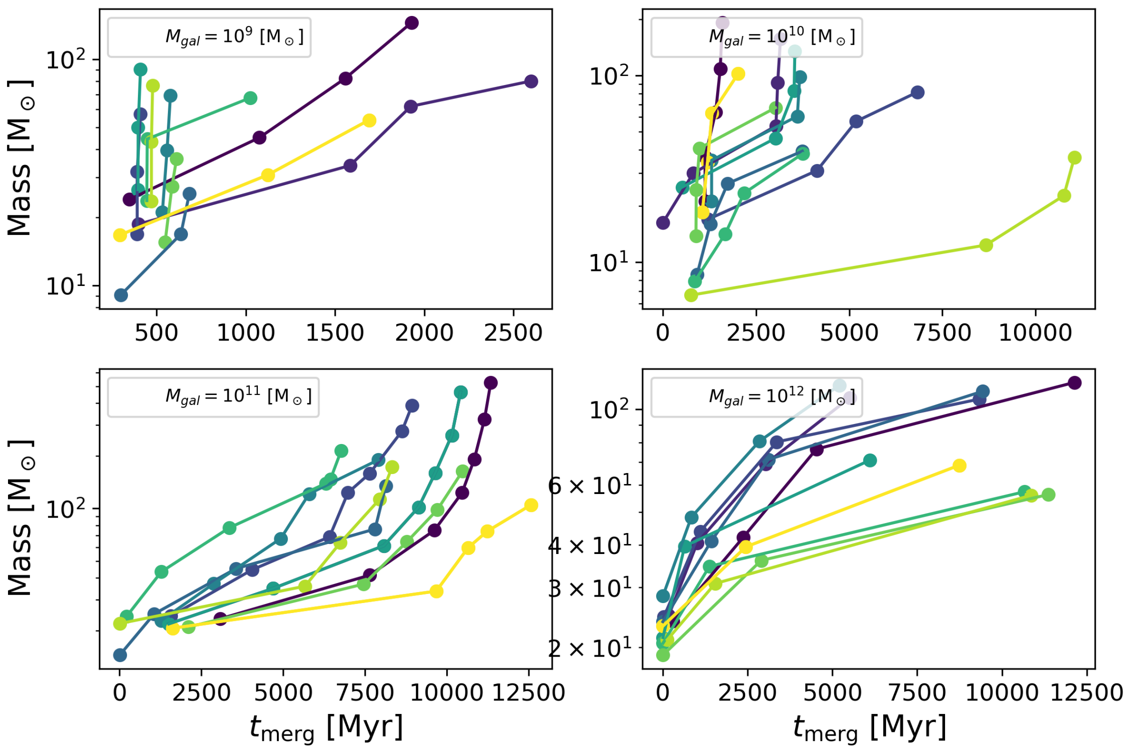

Figure 6.5: Merger Chain of BHs in cluster with local BHs.

Studying the merger chains of BH provide information on the dynamical time, which tell us about the NSCs they live in. Figure 6.5 shows merger chains of LL runs. In these four plots, I have selected ten merger chains among which six are random while four are for BHs that perform the most hierarchical mergers. In the first plot for $10^9 M_\odot$ galaxy, we see more than half the BHs performing runaway mergers. The longest a BH takes to inspiral and merge is

1 billion years. Another important fact to notice would be which BHs have merged. Most of them had masses above $10M_\odot$ and formation time greater than a few hundred million years. This is logical considering that the more massive a BH is, the smaller is the supernova kick. Simultaneously, the later a BH forms, heavier the NSC is and more is the escape velocity. An interesting fact is that in such light NSCs, hierarchical merger stops a couple of billion years after the star formation stops. So, for lighter NSCs to exhibit gravitational waves event in current epoch, it may have had a recent star formation episode.

On the other extreme, for $10^{12}M_\odot$ galaxy, as dynamical time is too long, we see long lines between two successive mergers. More massive BHs find it easier to merge due to their smaller dynamical and coalescence time. On the other hand, BHs formed at earlier times are more probable to merge since velocity dispersion is small in the beginning. If an NSC is extremely heavy and formed as soon as the first galaxies formed, there can still be merger happening in them from those early BHs.

As for $10^{10}M_\odot$ and $10^{11}M_\odot$ galaxy runs, the results are a mixture of both extreme, with the former preferring run-away mergers and later preferring long dynamical formations. In $10^{11}M_\odot$ plot, we see a hint of runaway mergers at the higher generations. If the BH mass is able to overcome the effect brought by velocity dispersion, we can form BHs heavier than a $1000M_\odot$.

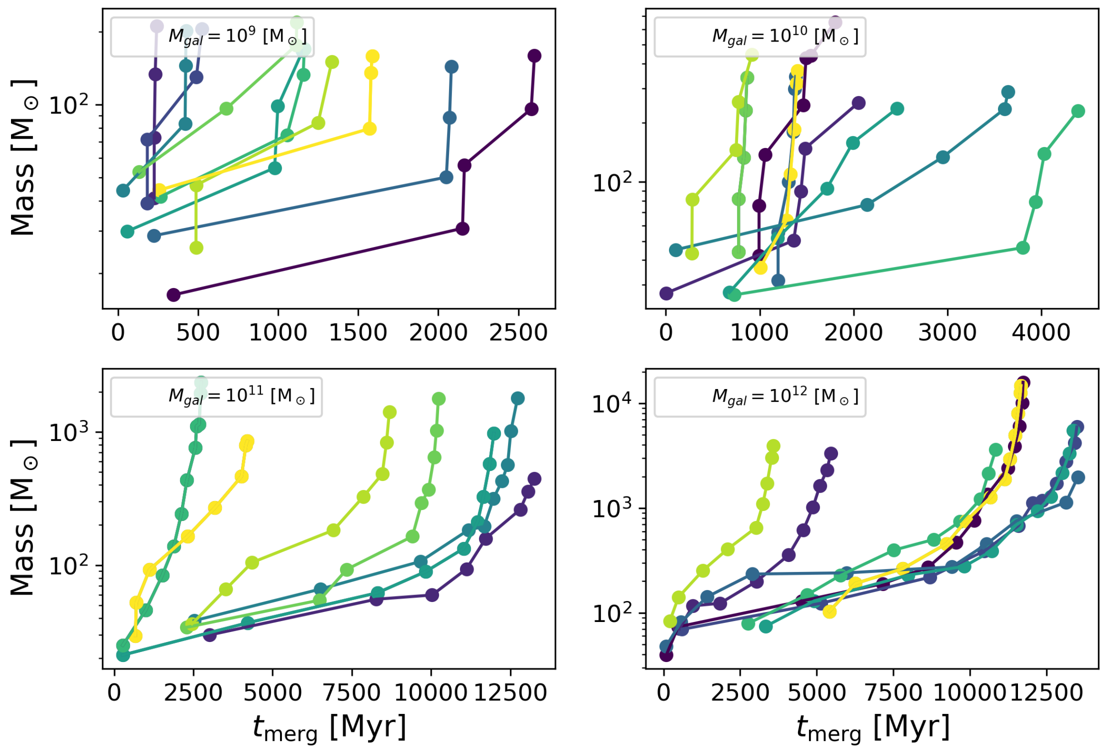

Figure 6.6: Merger Chain of BHs in cluster with accreting BHs in Late Type galaxy

In figure 6.6 showing the merger chains of LML run, we still observe the general trends, heavier mass BHs are more likely to merge. Lighter NSCs prefer BH formed later while heavier NSCs prefer BH formed earlier. However, with increased BH mass population, the second scenario is relaxed. In 10^{11} and $10^{12}M_\odot$ galaxies, we also see merger chains of BH formed later on. Another major difference would be runaway mergers in the heavier NSCs, capable of producing

BHs heavier than $1000 M_{\odot}$. If SMBHs are created from seed IMBHs, the probability of them to form in heaviest NSC is high, which in turn means the heaviest galaxies. This can be a reason for the creation of SMBHs in such galaxies and absence of NSCs in them.

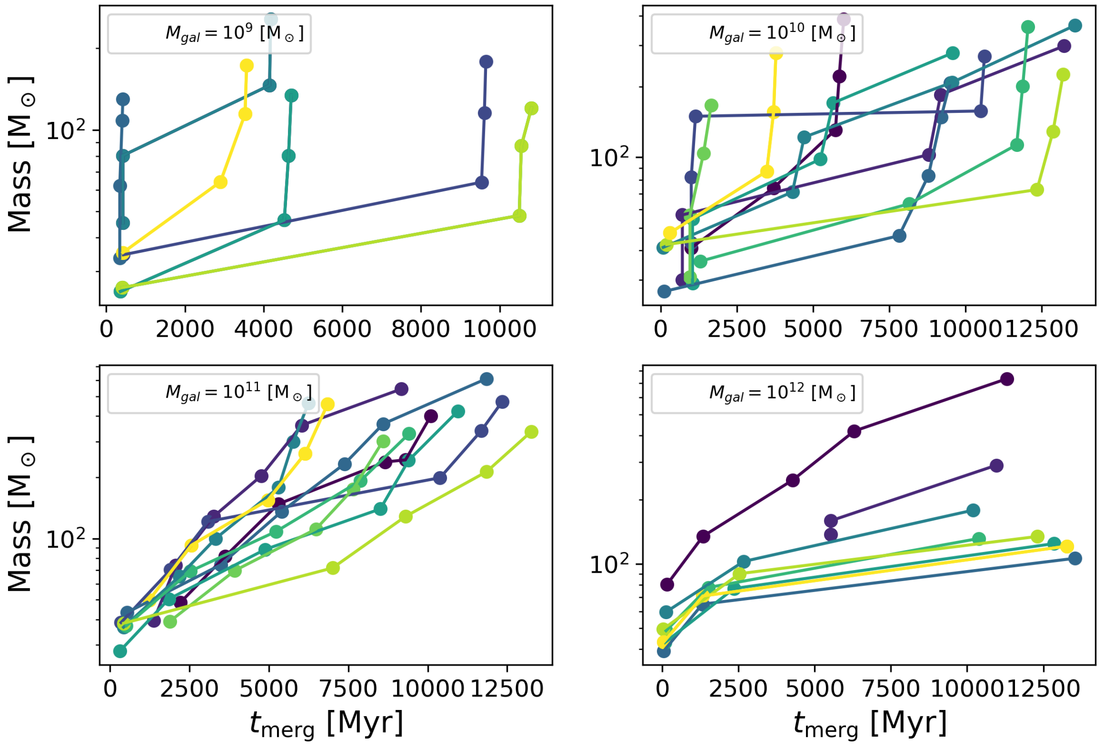

Figure 6.7: Merger Chain of BHs in cluster with accreting BHs in Early Type galaxy

Lastly, the merger chains of LME are shown in figure 6.7. The decrease in density makes runaway mergers in NSCs of all masses less likely. The lightest NSCs in $10^9 M_{\odot}$ galaxy run only have a few runaway mergers. Simultaneously, we get mergers chain that last more than ten billion years, something we hadn't seen previously.

6.5 Observational Comparison

Population of BHs from all our simulations can be seen in figure 6.8. The plots are of primary mass versus secondary mass of all merging BHs across the generations. The color scheme simply tells us what mass of BHs are merging more. The black points overlapped on the distribution are GW observational data from O1, O2, and O3 observational runs. The data is shown in appendix B. The elongated bars on each point are uncertainties of GW data.

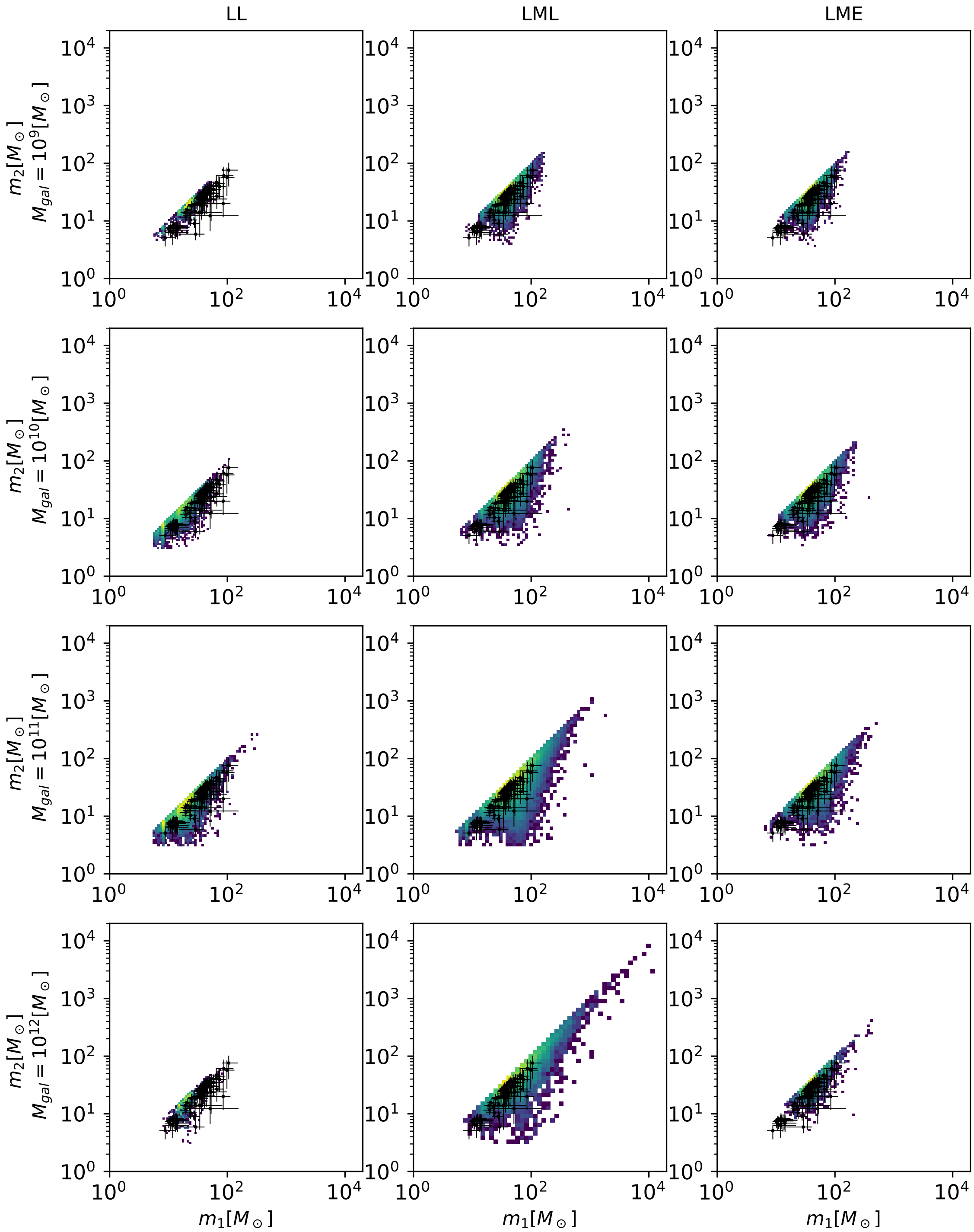

Figure 6.8: 2D histograms of primary and secondary mass of all the simulations. The color scheme tells us what mass of BHs are merging more likely. The black points overlapped on the distribution are GW observational data from O1, O2, and O3 observational runs. The data are shown in appendix B. The bars on each point are 90% uncertainties of GW data. The same plots without GW data is in appendix C

As we have already discussed in the previous sections, changing the initial mass population in LML runs has significantly altered the merging BH population. The difference can be clearly seen by comparing LL and LML models, we have more massive mergers in both LML and LME runs. The major difference in LML and LME shows up in heavier galaxies, with LME producing no BHs above a $1000M_{\odot}$.

It can be seen from the figure that LML and LME runs are capable of producing BH mergers in similar mass range of most of the GW events. While LL fails to reproduce BH mergers near the heaviest GW events. It also seems unlikely that the lower mass end GW events came from dynamical formation in NSCs.

The inability of LL run to reproduce the data can also be seen from figure 6.9, where I have plotted the final mass of the remnants along their spins.The effect is even more pronounced than mass distribution.

A trend to observe here is that with increasing mass, the spins also increase. It isn't straightforwards to see but can be inferred by watching the higher population of spins with increasing masses. In $10^{10}M_{\odot}$ and $10^{11}M_{\odot}$ runs of LML and LME, we can clearly see the yellow dense region shifting towards higher spins with increasing mass. Higher generation mergers produce higher spins remnants.

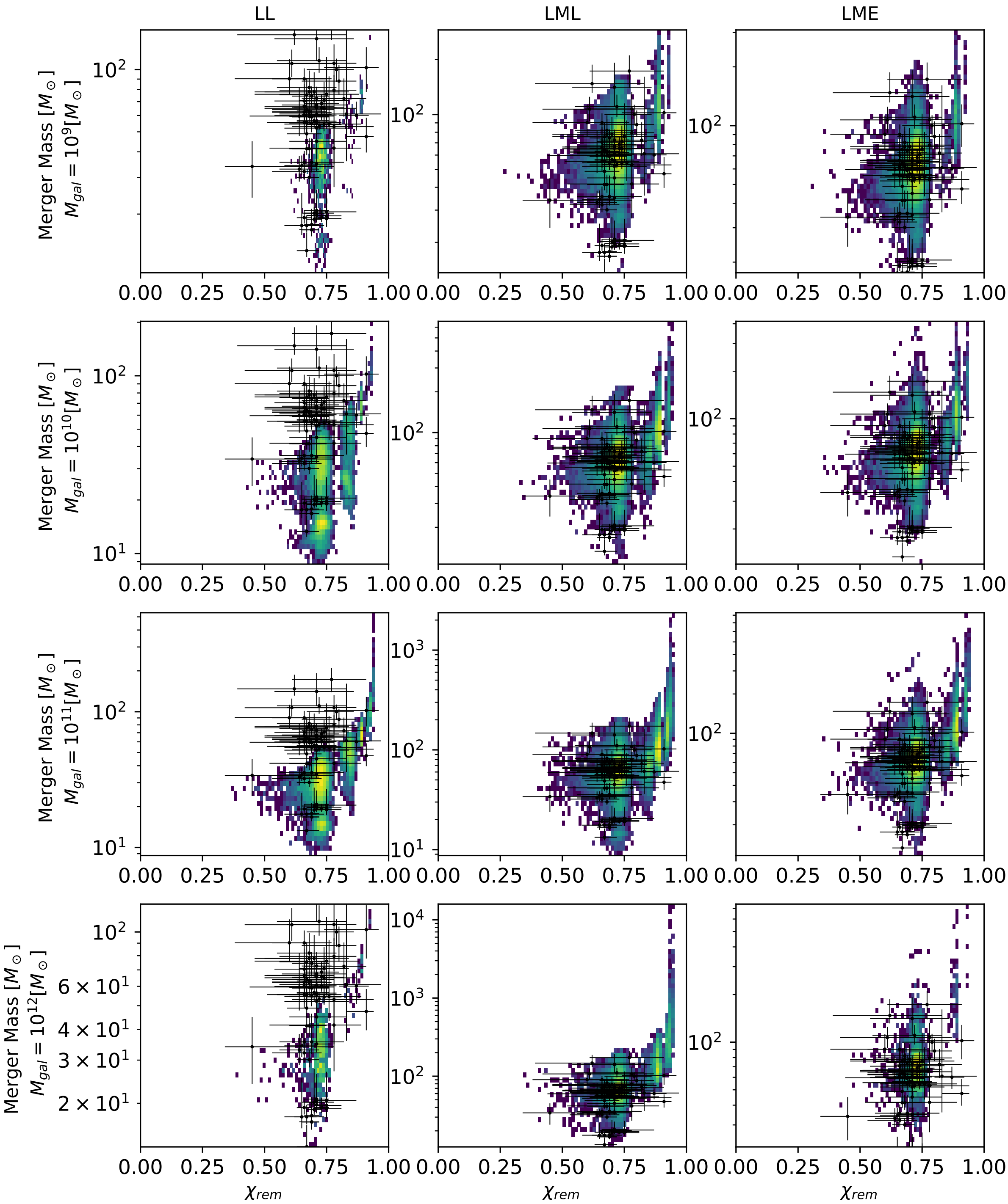

Figure 6.9: 2D histograms of remnant mass and remnant spins of all the simulations. The color scheme is similar to figure 6.8. The black points overlapped on the distribution are GW observational data from O1, O2, and O3 observational runs. The data are shown in appendix B. The bars on each point are 90% uncertainties of GW data. The same plots without GW data is in appendix C

Chapter 7

Conclusion and Future Work

We started our discussion with showing that dynamical formation of BBH could answer the inconsistency in BH mass distribution inferred from GW data. We could form BHs in pair-instability mass gap and even have these BHs form binaries through hierarchical mergers. NSC were excellent locations to study this phenomenon with high density and escape velocity. In this thesis, we wanted to study BBH mergers in a realistic NSC, which is growing through GC accretion. To study this phenomenon, we created a semi-analytical model for NSC evolution and matched it with observational data. Once we were sure our model worked nicely, we implemented it into FASTCLUSTER

We had to exhaustively update the FASTCLUSTER code to include our realistic model. Simultaneously, we created a BH library that could form in GC and stay within the cluster. We did this by running ten simulations of FASTCLUSTER in GC mode and selecting all the BHs that were not ejected by supernova, relativistic, or dynamical kicks.

We performed 12 simulations with 10^5 BHs. Depending on the initial BH mass population and galaxy type, we divided these 12 simulations into three groups named: Local BH and Late type galaxy (LL), Local BH, Migratory BH, and Late type galaxy (LML), and Local BH, Migratory BH, and Early type galaxy (LME). Each group was further divided by galaxy mass of 10^9, 10^{10}, 10^{11}, and $10^{12} M_\odot$. Local BH are produced in NSC while migratory BH come from GC accretion.

Through the results of LL simulations, we were able to answer an important question: are NSCs of all masses efficient in hierarchical mergers? In chapter 6, we found that although NSCs of all masses were capable of producing IMBHs, the lightest and heaviest NSCs couldn't go above three generations. In the lightest NSCs, small escape velocities caused most of the BHs to be ejected from the cluster. On the heaviest side, greater velocity dispersion caused longer formation and merger time for the binaries. We wouldn't see those mergers within Hubble time.

The LML simulations showed us how the initial BH population could alter the dynamics of BBH. With heavier BHs coming from GCs, we were able to shorten the dynamical time for forming and merging BHs. This effect was seen across the NSC masses with the greatest effect in the heaviest NSCs. In the heaviest NSCs, larger dynamical time was the reason behind halting of hierarchical mergers. With this problem solved, we were able to form BH with masses greater than $10000 M_\odot$ in the heaviest NSCs.

In chapter 3, we studied two formation channels of NSCs, asking if the formation channel affected BBH mergers inside. Indeed, with the GC migratory channel, we see a larger initial

BH population (LML) that significantly changes the BBH dynamics inside.

The formation of BHs larger than $2000M_\odot$ in late type galaxies of mass 10^{11} and $10^{12}M_\odot$ could answer the presence of SMBH in these galaxies. Such MBHs may be seeds that give birth to SMBHs in heavier galaxies. These SMBHs can disrupt the NSCs, leading to absence of NSCs in high mass galaxies. The SMBH can also co-exist with the NSCs like in our Milky Way and M31.

An important question was the impact of NSC's evolution on BBH dynamics. We saw from figures 6.5, 6.6, 6.7 that in many simulations, the evolution of NSC created an increase in dynamical time. In simulations where the increase in BH mass was able to overcome the evolution's effects, we saw run-away mergers of BHs. Additionally, we saw that in the lightest NSCs, most of BBH mergers stop after a few billion years of NSCs formation.

In LME simulations, we changed the galaxy type to early, which created bigger NSCs in size. Greater sizes for similar masses meant smaller densities, which changed the dynamical times for BBH formation and merger. Despite a heavier BH population coming from GCs, we weren't able to produce BHs greater than a $1000M_\odot$. According to our model and analysis, SMBH creation in massive early type galaxies seems unlikely from seed IMBHs. We know from chapter 3 that most massive early type galaxy do not host NSCs and host SMBHs. Our model is unable to answer this question.

Lastly, we compared the results we obtained from our simulations with confident GW detections from GWTC-1,2, and 3 (figure 6.8). We found that it is highly unlikely that these observations came from BHs that formed in NSCs. They have small masses and longer dynamical time to form hierarchical mergers of heavier mass. On the other hand, LML and LME simulations showed that they can produce mergers similar to GW events. These effects can also be seen in figure 6.9.

To conclude, the physical properties of NSC along with its formation channel, and evolution affect the dynamics of BBHs inside. Conversely, BBH detection from NSCs can shed light on NSC formation and evolution processes, which is still an active area of research.

This work is the first step towards a more refined FASTCLUSTER code that could reproduce the physical phenomenon more precisely. The GC migratory model we consider for NSC evolution has room for growth. First, we have only considered GCs within the scale length. In lighter galaxy cases, the GC within scale length inspiral to the NSC within just a few million years. But the accretion doesn't stop there. We will account for this in the future. Secondly, there is no consideration for tidal forces that disrupt the GCs. This is important since it will alter the growth trajectory of the NSCs, certainly in the heaviest galaxies.

The BH libraries we took for both local and migratory BH were from evolution of stars around solar metallicity. This is not exactly true for GCs who show older population stars and thus lower metallicity. GCs can also produce heavier mass BH from stellar evolution that we haven't considered. The change in metallicity will change the initial BH mass population, thus heavily altering the final BBH population.

Appendices

Appendix A

Coalescence

When two stellar bodies revolve around each other, they create ripples in the fabric of space-time that propagate in the form of gravitational waves. These waves carry away the energy from the system, causing the binary to shrink and eventually merge. From linearized Einstein's equations, we know that an object with stress energy tensor $T_{\mu\nu}$ can act produce small perturbations,

$$\Box h_{\mu\nu} = -\frac{2T_{\mu\nu}}{M_p}, \tag{A.1}$$

where M_p is the reduced Planck mass. In vacuum, these equations reduce to a four-dimensional analog of wave equations, easily solved by a sinusoidal system. But what we are interested is knowing the waves emitted by a binary system. Solving this equation in its grandness is not the aim of this thesis, so I will simply skip to the main results. For a system to two bodies orbiting each other, the perturbation created is,

$$\begin{aligned} h_+(t,\theta,\phi) &= \frac{1}{r}\frac{4G^{5/3}\omega_S^{2/3}\mu M^{2/3}}{c^4}\frac{1+\cos^2\theta}{2}\cos(2\omega_s t + 2\phi) \\ h_\times(t,\theta,\phi) &= \frac{1}{r}\frac{4G^{5/3}\omega_S^{2/3}\mu M^{2/3}}{c^4}\cos(\theta)\sin(2\omega_s t + 2\phi) \end{aligned} \tag{A.2}$$

h_+ and $h_\times$ are two polarization of the gravitational waves seen by an observer present in the direction of (θ, ϕ). μ is the reduced mass of the system while M is the total mass. It can be seen that depending on where the observer is, the amplitude of gravitational waves can change, which greatly helps in localizing these waves from observations. These waves naturally carry away some energy, which can be inferred by inverting Einstein's equations. The total radiated power is,

$$\dot{E}_{GW} = \frac{dE}{dt} = \frac{32}{5}\frac{c^5}{G}\left(\frac{GM_c\omega_{GW}}{2c^3}\right)^{10/3}, \tag{A.3}$$

where M_c is the chirp mass, defined as $M_c = \mu^{3/5}M^{2/5}$. Ignoring the constants, we can easily see that for large mass bodies, the energy released as GW is also large. The same could be said about the frequency. The faster those bodies rotate, the more energy per unit time they emit.

A two body system, virialized has its total energy just half the potential energy,

$$E = \frac{Gm_1m_2}{2R}. \tag{A.4}$$

The change in energy brought by the change in radius is,

$$\dot{E} = -\frac{Gm_1m_2}{2R^2}\dot{R}. \tag{A.5}$$

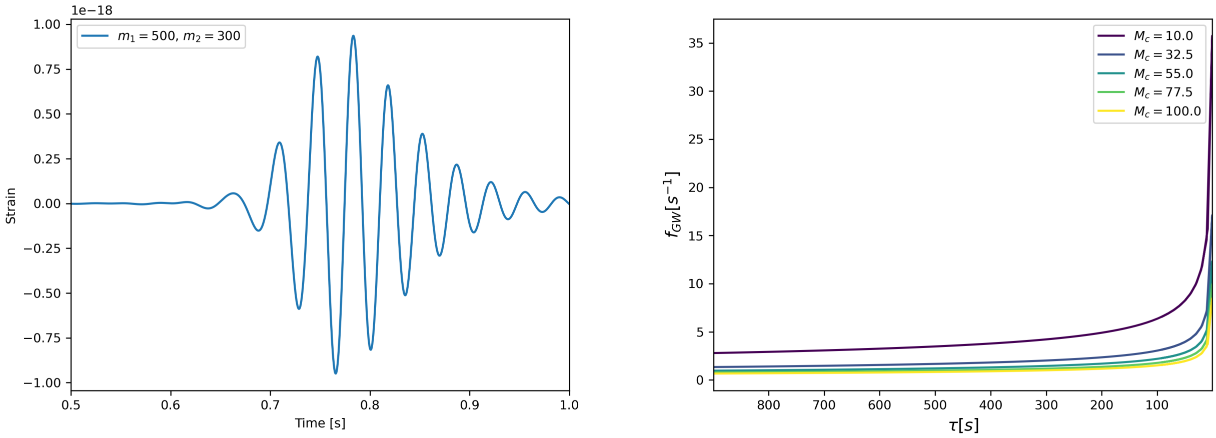

Figure A.1: Left: Chirping Waveform created using pycbc package. $m_1 = 500M_\odot$, $m_2 = 300M_\odot$,$S_1 = 0.9$,$S_2 = 0.4$ and $e = 0$ are the physical parameters of the binary taken to form this waveform. Right: The evolution of frequency according to equation A.10 for various mass combination of primary and secondary. We see that for our frequency of interest (10Hz), most binaries come into this range only towards the end of their life, the final few seconds.

From Kepler's third law, we find an equation connecting radius with angular frequency,

$$R = \left(\frac{GM}{\omega_s^2}\right)^{1/3} \tag{A.6}$$

Differentiating and solving, we find,

$$\dot{R} = -\frac{2}{3}\frac{\dot{\omega}_s}{\omega_s}R \tag{A.7}$$

Combining equations (A.3),(A.5),(A.7), we arrive at the result,

$$\dot{\omega}_{GW} = \frac{12(2)^{1/3}}{5}\left(\frac{GM_c}{c^3}\right)^{5/3}\omega_{GW}^{11/3}, \qquad \text{where} \qquad \omega_s = 2\omega_{GW} \tag{A.8}$$

or

$$\begin{aligned} \dot{f}_{GW} &= \frac{96}{5}\pi^{8/3}\left(\frac{GM_c}{c^3}\right)^{5/3} f_{GW}^{11/3} \\ \dot{f}_{GW} &= k f_{GW} \end{aligned} \tag{A.9}$$

Above equation can be easily solved to give us the final result of,

$$f_{GW} = \frac{1}{\pi}\left(\frac{5}{256\tau}\right)^{3/8}\left(\frac{c^3}{GM_c}\right)^{5/8}, \tag{A.10}$$

where $\tau = t - t_{coal}$ and t_{coal} is the time of merger. Inverting the above equation can give us the time for merger,

$$\tau = \frac{5}{256}\left(\frac{1}{\pi f_{GW}}\right)^{8/3}\left(\frac{c^3}{GM_c}\right)^{5/3}, \tag{A.11}$$

Appendix B

GW Observations

Table B.1: GW data for BBHs from O1,O2, and O3 runs.

GW Event -	Primary Mass $M_\odot$	Secondary Mass $M_\odot$	χ_{eff} -	Remnant Mass $M_\odot$
GW150914	$35.6^{4.7}_{-3.1}$	$30.6^{3.0}_{-4.4}$	$-0.01^{0.12}_{-0.13}$	$63.1^{3.4}_{-3.0}$
GW151012	$23.2^{14.9}_{-5.5}$	$13.6^{4.1}_{-4.8}$	$0.05^{0.31}_{-0.2}$	$35.6^{10.8}_{-3.8}$
GW151226	$13.7^{8.8}_{-3.2}$	$7.7^{2.2}_{-2.5}$	$0.18^{0.2}_{-0.12}$	$20.5^{6.4}_{-1.5}$
GW170104	$30.8^{7.3}_{-5.6}$	$20.0^{4.9}_{-4.6}$	$-0.04^{0.17}_{-0.21}$	$48.9^{5.1}_{-4.0}$
GW170608	$11.0^{5.5}_{-1.7}$	$7.6^{1.4}_{-2.2}$	$0.03^{0.19}_{-0.07}$	$17.8^{3.4}_{-0.7}$
GW170729	$50.2^{16.2}_{-10.2}$	$34.0^{9.1}_{-10.1}$	$0.37^{0.21}_{-0.25}$	$79.5^{14.7}_{-10.2}$
GW170809	$35.0^{8.3}_{-5.9}$	$23.8^{5.1}_{-5.2}$	$0.08^{0.17}_{-0.17}$	$56.3^{5.2}_{-3.8}$
GW170814	$30.6^{5.6}_{-3.0}$	$25.2^{2.8}_{-4.0}$	$0.07^{0.12}_{-0.12}$	$53.2^{3.2}_{-2.4}$
GW170818	$35.4^{7.5}_{-4.7}$	$26.7^{4.3}_{-5.2}$	$-0.09^{0.18}_{-0.21}$	$59.4^{4.9}_{-3.8}$
GW170823	$39.5^{11.2}_{-6.7}$	$29.0^{6.7}_{-7.8}$	$0.09^{0.22}_{-0.26}$	$65.4^{10.1}_{-7.4}$
GW190403_051519	$85.0^{27.8}_{-33.0}$	$20.0^{26.3}_{-8.4}$	$0.68^{0.16}_{-0.43}$	$102.2^{26.3}_{-24.3}$
GW190408_181802	$24.8^{5.4}_{-3.5}$	$18.5^{3.3}_{-4.0}$	$-0.03^{0.13}_{-0.17}$	$41.4^{3.9}_{-2.9}$
GW190412	$27.7^{6.0}_{-6.0}$	$9.0^{2.0}_{-1.4}$	$0.21^{0.12}_{-0.13}$	$35.6^{4.8}_{-4.5}$
GW190413_052954	$33.7^{10.4}_{-6.4}$	$24.2^{6.5}_{-7.0}$	$-0.04^{0.27}_{-0.32}$	$55.5^{10.1}_{-7.3}$
GW190413_134308	$51.3^{16.6}_{-12.6}$	$30.4^{11.7}_{-12.7}$	$-0.01^{0.28}_{-0.38}$	$78.0^{16.1}_{-11.5}$
GW190421_213856	$42.0^{10.1}_{-7.4}$	$32.0^{8.3}_{-9.8}$	$-0.1^{0.21}_{-0.27}$	$70.5^{12.4}_{-9.0}$
GW190426_190642	$105.5^{45.3}_{-24.1}$	$76.0^{26.2}_{-36.5}$	$0.23^{0.42}_{-0.41}$	$172.9^{37.7}_{-33.6}$
GW190503_185404	$41.3^{10.3}_{-7.7}$	$28.3^{7.5}_{-9.2}$	$-0.05^{0.23}_{-0.3}$	$66.5^{9.4}_{-7.9}$
GW190512_180714	$23.2^{5.6}_{-5.6}$	$12.5^{3.5}_{-2.6}$	$0.02^{0.13}_{-0.14}$	$34.3^{4.1}_{-3.4}$
GW190513_205428	$36.0^{10.6}_{-9.7}$	$18.3^{7.4}_{-4.7}$	$0.16^{0.29}_{-0.22}$	$52.1^{8.8}_{-6.6}$
GW190514_065416	$40.9^{17.3}_{-9.3}$	$28.4^{10.0}_{-10.1}$	$-0.08^{0.29}_{-0.35}$	$66.4^{19.0}_{-11.5}$
GW190517_055101	$39.2^{13.9}_{-9.2}$	$24.0^{7.4}_{-7.9}$	$0.49^{0.21}_{-0.28}$	$60.1^{9.9}_{-9.4}$
GW190519_153544	$65.1^{10.8}_{-11.0}$	$40.8^{11.5}_{-12.7}$	$0.33^{0.2}_{-0.24}$	$100.0^{13.0}_{-12.9}$
GW190521	$98.4^{33.6}_{-21.7}$	$57.2^{27.1}_{-30.1}$	$-0.14^{0.5}_{-0.45}$	$147.4^{40.0}_{-16.0}$
GW190521_074359	$43.4^{5.8}_{-5.5}$	$33.4^{5.2}_{-6.8}$	$0.1^{0.13}_{-0.13}$	$72.6^{6.5}_{-5.4}$
GW190527_092055	$35.6^{18.7}_{-8.0}$	$22.2^{9.0}_{-8.7}$	$0.1^{0.22}_{-0.22}$	$55.5^{17.9}_{-8.5}$
GW190602_175927	$71.8^{18.1}_{-14.6}$	$44.8^{15.5}_{-19.6}$	$0.12^{0.25}_{-0.28}$	$110.5^{17.9}_{-13.9}$
GW190620_030421	$58.0^{19.2}_{-13.3}$	$35.0^{13.1}_{-14.5}$	$0.34^{0.22}_{-0.29}$	$88.0^{17.2}_{-12.4}$
GW190630_185205	$35.1^{6.5}_{-5.5}$	$24.0^{5.5}_{-5.2}$	$0.1^{0.14}_{-0.13}$	$56.6^{4.4}_{-4.5}$
GW190701_203306	$54.1^{12.6}_{-8.0}$	$40.5^{8.7}_{-12.1}$	$-0.08^{0.23}_{-0.31}$	$90.2^{11.2}_{-8.9}$
GW190706_222641	$74.0^{20.1}_{-16.9}$	$39.4^{18.4}_{-15.4}$	$0.28^{0.25}_{-0.31}$	$107.3^{25.2}_{-15.9}$
GW190707_093326	$12.1^{2.6}_{-2.0}$	$7.9^{1.6}_{-1.3}$	$-0.04^{0.1}_{-0.09}$	$19.2^{1.7}_{-1.2}$

Continued on next page

Table B.1 – continued from previous page

GW Event -	Primary Mass $M_{\odot}$	Secondary Mass $M_{\odot}$	χ_{eff} -	Remnant Mass $M_{\odot}$
GW190708_232457	$19.8^{4.3}_{-4.3}$	$11.6^{3.1}_{-2.0}$	$0.05^{0.1}_{-0.1}$	$30.1^{2.9}_{-2.1}$
GW190719_215514	$36.6^{42.1}_{-11.1}$	$19.9^{10.0}_{-9.3}$	$0.25^{0.33}_{-0.32}$	$54.5^{38.3}_{-11.1}$
GW190720_000836	$14.2^{5.6}_{-3.3}$	$7.5^{2.2}_{-1.8}$	$0.19^{0.14}_{-0.11}$	$20.8^{3.9}_{-2.0}$
GW190725_174728	$11.8^{10.1}_{-3.0}$	$6.3^{2.1}_{-2.5}$	$-0.04^{0.36}_{-0.16}$	$17.6^{7.7}_{-1.8}$
GW190727_060333	$38.9^{8.9}_{-6.0}$	$30.2^{6.5}_{-8.3}$	$0.09^{0.25}_{-0.27}$	$65.4^{9.5}_{-7.3}$
GW190728_064510	$12.5^{6.9}_{-2.3}$	$8.0^{1.7}_{-2.6}$	$0.13^{0.19}_{-0.07}$	$19.7^{4.4}_{-1.4}$
GW190731_140936	$41.8^{12.7}_{-9.1}$	$29.0^{10.2}_{-9.9}$	$0.07^{0.28}_{-0.25}$	$67.4^{15.3}_{-10.8}$
GW190803_022701	$37.7^{9.8}_{-6.7}$	$27.6^{7.6}_{-8.5}$	$-0.01^{0.23}_{-0.28}$	$62.1^{11.2}_{-7.6}$
GW190805_211137	$46.2^{15.4}_{-11.2}$	$30.6^{11.8}_{-11.3}$	$0.37^{0.29}_{-0.39}$	$72.4^{18.2}_{-13.2}$
GW190828_063405	$31.9^{5.4}_{-4.1}$	$25.8^{4.9}_{-5.3}$	$0.15^{0.15}_{-0.16}$	$54.3^{7.3}_{-4.0}$
GW190828_065509	$23.7^{6.8}_{-6.7}$	$10.4^{3.8}_{-2.2}$	$0.05^{0.16}_{-0.17}$	$33.0^{5.3}_{-4.3}$
GW190910_112807	$43.8^{7.6}_{-6.8}$	$34.2^{6.6}_{-7.3}$	$0.0^{0.17}_{-0.2}$	$74.4^{8.5}_{-8.6}$
GW190915_235702	$32.6^{8.8}_{-4.9}$	$24.5^{4.9}_{-5.8}$	$-0.03^{0.19}_{-0.24}$	$54.7^{6.6}_{-5.0}$
GW190916_200658	$43.8^{19.9}_{-12.6}$	$23.3^{12.5}_{-10.0}$	$0.2^{0.33}_{-0.31}$	$65.0^{17.3}_{-12.6}$
GW190924_021846	$8.8^{4.3}_{-1.8}$	$5.1^{1.2}_{-1.5}$	$0.03^{0.2}_{-0.08}$	$13.3^{3.0}_{-0.9}$
GW190925_232845	$20.8^{6.5}_{-2.9}$	$15.5^{2.5}_{-3.6}$	$0.09^{0.16}_{-0.15}$	$34.9^{3.5}_{-2.6}$
GW190926_050336	$41.1^{20.8}_{-12.5}$	$20.4^{11.4}_{-8.2}$	$-0.02^{0.25}_{-0.32}$	$59.6^{22.1}_{-11.8}$
GW190929_012149	$66.3^{21.6}_{-16.6}$	$26.8^{14.7}_{-10.6}$	$-0.03^{0.23}_{-0.28}$	$90.3^{22.3}_{-14.6}$
GW190930_133541	$14.2^{8.0}_{-4.0}$	$6.9^{2.4}_{-2.1}$	$0.19^{0.22}_{-0.16}$	$20.2^{6.1}_{-2.0}$
GW191103_012549	$11.8^{6.2}_{-2.2}$	$7.9^{1.7}_{-2.4}$	$0.21^{0.16}_{-0.1}$	$19.0^{3.8}_{-1.7}$
GW191105_143521	$10.7^{3.7}_{-1.6}$	$7.7^{1.4}_{-1.9}$	$-0.02^{0.13}_{-0.09}$	$17.6^{2.1}_{-1.2}$
GW191109_010717	$65.0^{11.0}_{-11.0}$	$47.0^{15.0}_{-13.0}$	$-0.29^{0.42}_{-0.31}$	$107.0^{18.0}_{-15.0}$
GW191113_071753	$29.0^{12.0}_{-14.0}$	$5.9^{4.4}_{-1.3}$	$0.0^{0.37}_{-0.29}$	$34.0^{11.0}_{-10.0}$
GW191126_115259	$12.1^{5.5}_{-2.2}$	$8.3^{1.9}_{-2.4}$	$0.21^{0.15}_{-0.11}$	$19.6^{3.5}_{-2.0}$
GW191127_050227	$53.0^{47.0}_{-20.0}$	$24.0^{17.0}_{-14.0}$	$0.18^{0.34}_{-0.36}$	$76.0^{39.0}_{-21.0}$
GW191129_134029	$10.7^{4.1}_{-2.1}$	$6.7^{1.5}_{-1.7}$	$0.06^{0.16}_{-0.08}$	$16.8^{2.5}_{-1.2}$
GW191204_110529	$27.3^{11.0}_{-6.0}$	$19.3^{5.6}_{-6.0}$	$0.05^{0.26}_{-0.27}$	$45.0^{8.6}_{-7.6}$
GW191204_171526	$11.9^{3.3}_{-1.8}$	$8.2^{1.4}_{-1.6}$	$0.16^{0.08}_{-0.05}$	$19.21^{1.79}_{-0.95}$
GW191215_223052	$24.9^{7.1}_{-4.1}$	$18.1^{3.8}_{-4.1}$	$-0.04^{0.17}_{-0.21}$	$41.4^{5.1}_{-4.1}$
GW191216_213338	$12.1^{4.6}_{-2.3}$	$7.7^{1.6}_{-1.9}$	$0.11^{0.13}_{-0.06}$	$18.87^{2.8}_{-0.94}$
GW191222_033537	$45.1^{10.9}_{-8.0}$	$34.7^{9.3}_{-10.5}$	$-0.04^{0.2}_{-0.25}$	$75.5^{15.3}_{-9.9}$
GW191230_180458	$49.4^{14.0}_{-9.6}$	$37.0^{11.0}_{-12.0}$	$-0.05^{0.26}_{-0.31}$	$82.0^{17.0}_{-11.0}$
GW200112_155838	$35.6^{6.7}_{-4.5}$	$28.3^{4.4}_{-5.9}$	$0.06^{0.15}_{-0.15}$	$60.8^{5.3}_{-4.3}$
GW200128_022011	$42.2^{11.6}_{-8.1}$	$32.6^{9.5}_{-9.2}$	$0.12^{0.24}_{-0.25}$	$71.0^{16.0}_{-11.0}$
GW200129_065458	$34.5^{9.9}_{-3.2}$	$28.9^{3.4}_{-9.3}$	$0.11^{0.11}_{-0.16}$	$60.3^{4.0}_{-3.3}$
GW200202_154313	$10.1^{3.5}_{-1.4}$	$7.3^{1.1}_{-1.7}$	$0.04^{0.13}_{-0.06}$	$16.76^{1.87}_{-0.66}$
GW200208_130117	$37.8^{9.2}_{-6.2}$	$27.4^{6.1}_{-7.4}$	$-0.07^{0.22}_{-0.27}$	$62.5^{7.3}_{-6.4}$
GW200208_222617	$51.0^{104.0}_{-30.0}$	$12.3^{9.0}_{-5.7}$	$0.45^{0.43}_{-0.44}$	$61.0^{100.0}_{-25.0}$
GW200209_085452	$35.6^{10.5}_{-6.8}$	$27.1^{7.8}_{-7.8}$	$-0.12^{0.24}_{-0.3}$	$59.9^{13.1}_{-8.9}$
GW200216_220804	$51.0^{22.0}_{-13.0}$	$30.0^{14.0}_{-16.0}$	$0.1^{0.34}_{-0.36}$	$78.0^{19.0}_{-13.0}$
GW200219_094415	$37.5^{10.1}_{-6.9}$	$27.9^{7.4}_{-8.4}$	$-0.08^{0.23}_{-0.29}$	$62.2^{11.7}_{-7.8}$
GW200220_061928	$87.0^{40.0}_{-23.0}$	$61.0^{26.0}_{-25.0}$	$0.06^{0.4}_{-0.38}$	$141.0^{51.0}_{-31.0}$
GW200220_124850	$38.9^{14.1}_{-8.6}$	$27.9^{9.2}_{-9.0}$	$-0.07^{0.27}_{-0.33}$	$64.0^{16.0}_{-11.0}$
GW200224_222234	$40.0^{6.9}_{-4.5}$	$32.5^{5.0}_{-7.2}$	$0.1^{0.15}_{-0.15}$	$68.6^{6.6}_{-4.7}$
GW200225_060421	$19.3^{5.0}_{-3.0}$	$14.0^{2.8}_{-3.5}$	$-0.12^{0.17}_{-0.28}$	$32.1^{3.5}_{-2.8}$
GW200302_015811	$37.8^{8.7}_{-8.5}$	$20.0^{8.1}_{-5.7}$	$0.01^{0.25}_{-0.26}$	$55.5^{8.9}_{-6.6}$

Continued on next page

Table B.1 – continued from previous page

GW Event -	**Primary Mass** $M_\odot$	**Secondary Mass** $M_\odot$	χ_{eff} -	**Remnant Mass** $M_\odot$
GW200306_093714	$28.3^{17.1}_{-7.7}$	$14.8^{6.5}_{-6.4}$	$0.32^{0.28}_{-0.46}$	$41.7^{12.3}_{-6.9}$
GW200308_173609	$36.4^{11.2}_{-9.6}$	$13.8^{7.2}_{-3.3}$	$0.65^{0.17}_{-0.21}$	$47.4^{11.1}_{-7.7}$
GW200311_115853	$34.2^{6.4}_{-3.8}$	$27.7^{4.1}_{-5.9}$	$-0.02^{0.16}_{-0.2}$	$59.0^{4.8}_{-3.9}$
GW200316_215756	$13.1^{10.2}_{-2.9}$	$7.8^{1.9}_{-2.9}$	$0.13^{0.27}_{-0.1}$	$20.2^{7.4}_{-1.9}$
GW200322_091133	$34.0^{48.0}_{-18.0}$	$14.0^{16.8}_{-8.7}$	$0.24^{0.45}_{-0.51}$	$53.0^{38.0}_{-26.0}$

Appendix C

Additional Figures

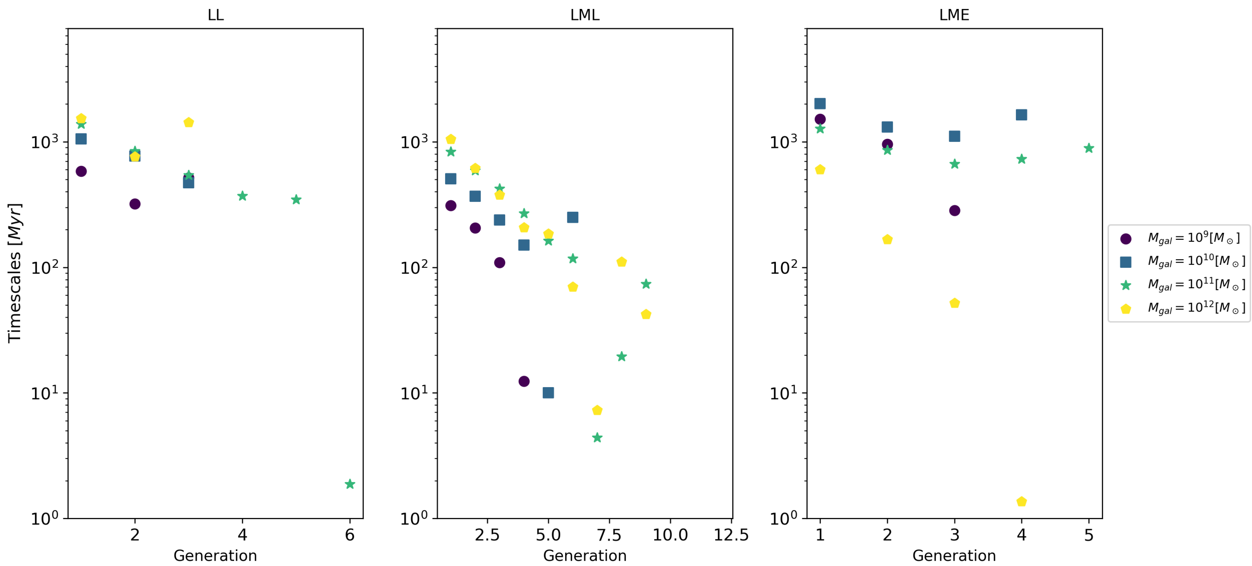

Figure C.1: Coalescence timescales for all the 12 simulations. The three subplots are of three major runs while the different color markers are for different galaxies. The points shown here are the average for all the BHs within that generation. We see that with each generation, coalescence time is generally decreasing.

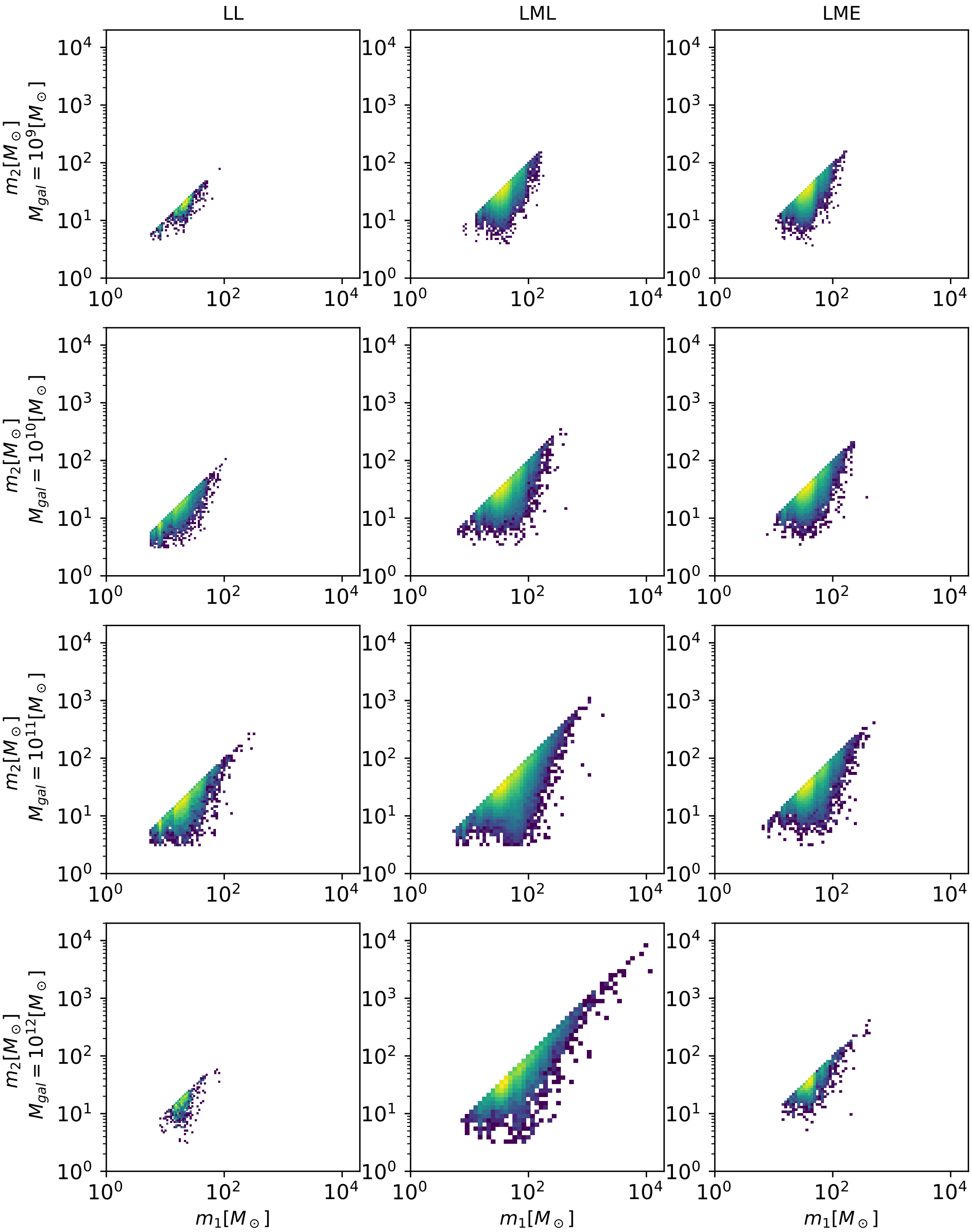

Figure C.2: 2D histograms of primary mass and secondary mass of all the simulations. The color scheme is similar to figure 6.8.

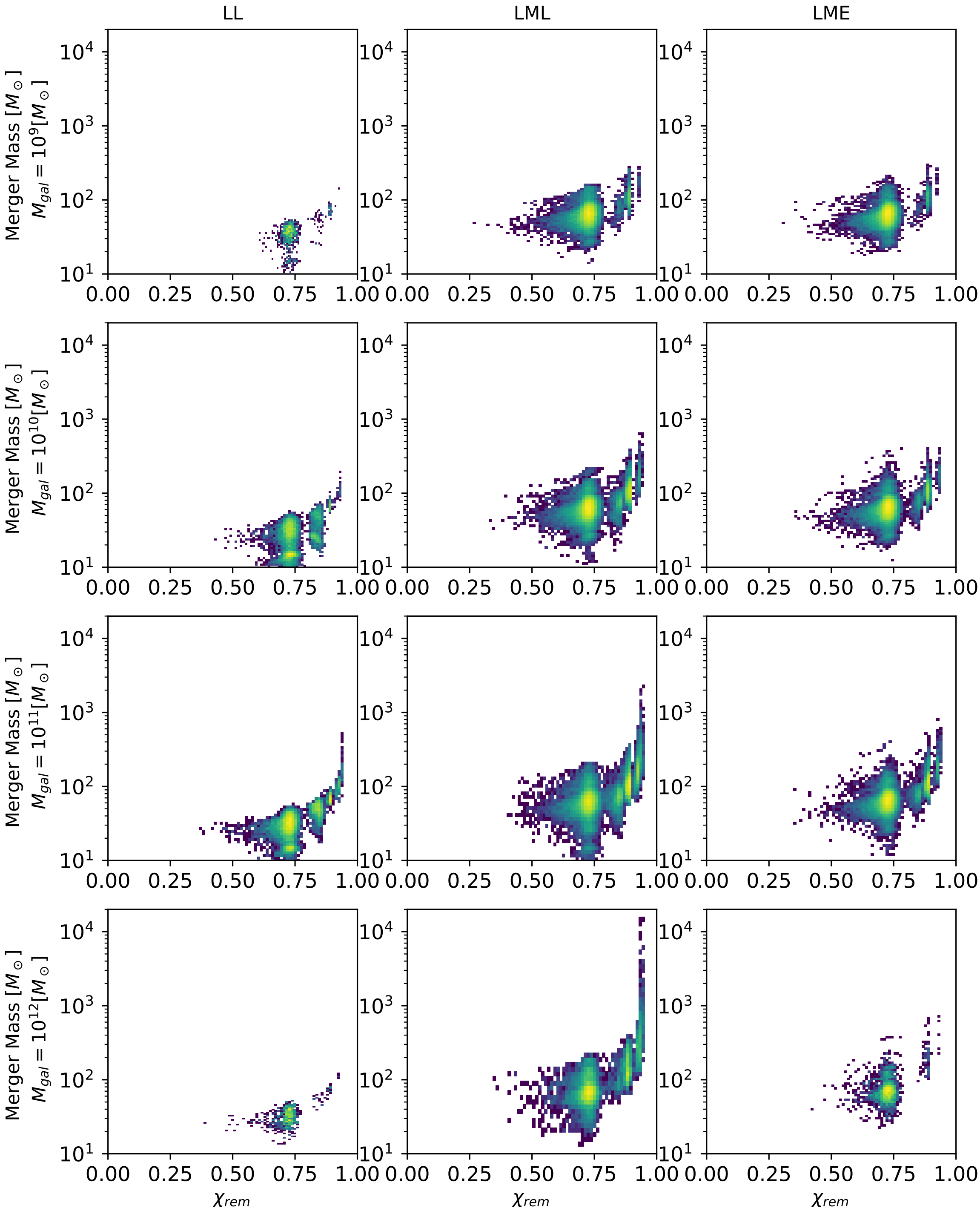

Figure C.3: 2D histograms of remnant mass and remnant spins of all the simulations. The color scheme is similar to figure 6.8.

Bibliography

Michela Mapelli. Astrophysics of stellar black holes. *Proc. Int. Sch. Phys. Fermi*, 200:87–121, 2020.

Nadine Neumayer, Anil Seth, and Torsten Böker. Nuclear star clusters. *The Astronomy and Astrophysics Review*, 28:1–75, 2020.

Iskren Y Georgiev, Torsten Böker, Nathan Leigh, Nora Lützgendorf, and Nadine Neumayer. Masses and scaling relations for nuclear star clusters, and their co-existence with central black holes. *Monthly Notices of the Royal Astronomical Society*, 457(2):2122–2138, 2016.

Benjamin P Abbott, Richard Abbott, TD Abbott, MR Abernathy, Fausto Acernese, Kendall Ackley, Carl Adams, Thomas Adams, Paolo Addesso, RX Adhikari, et al. Observation of gravitational waves from a binary black hole merger. *Physical review letters*, 116(6):061102, 2016.

R Abbott, TD Abbott, F Acernese, K Ackley, C Adams, N Adhikari, RX Adhikari, VB Adya, C Affeldt, D Agarwal, et al. Gwtc-3: compact binary coalescences observed by ligo and virgo during the second part of the third observing run. *arXiv preprint arXiv:2111.03606*, 2021.

Michela Mapelli, Marco Dall'Amico, Yann Bouffanais, Nicola Giacobbo, Manuel Arca Sedda, M Celeste Artale, Alessandro Ballone, Ugo N Di Carlo, Giuliano Iorio, Filippo Santoliquido, et al. Hierarchical black hole mergers in young, globular and nuclear star clusters: the effect of metallicity, spin and cluster properties. *Monthly Notices of the Royal Astronomical Society*, 505(1):339–358, 2021.

CJ Walcher, RP Van Der Marel, D McLaughlin, H-W Rix, T Böker, N Häring, LC Ho, M Sarzi, and JC Shields. Masses of star clusters in the nuclei of bulgeless spiral galaxies. *The Astrophysical Journal*, 618(1):237, 2005.

Nikolay Kacharov, Nadine Neumayer, Anil C Seth, Michele Cappellari, Richard McDermid, C Jakob Walcher, and Torsten Böker. Stellar populations and star formation histories of the nuclear star clusters in six nearby galaxies. *Monthly Notices of the Royal Astronomical Society*, 480(2):1973–1998, 2018.

Jennifer M Lotz, Rosemary Telford, Henry C Ferguson, Bryan W Miller, Massimo Stiavelli, and Jennifer Mack. Dynamical friction in de globular cluster systems. *The Astrophysical Journal*, 552(2):572, 2001.

Roberto Capuzzo-Dolcetta and Alessandra Mastrobuono-Battisti. Globular cluster system erosion in elliptical galaxies. *Astronomy & Astrophysics*, 507(1):183–193, 2009.

Scott D Tremaine, JP Ostriker, and L Spitzer Jr. The formation of the nuclei of galaxies. i-m31. *The Astrophysical Journal*, 196:407–411, 1975.

Manuel Arca-Sedda and Roberto Capuzzo-Dolcetta. The globular cluster migratory origin of nuclear star clusters. *Monthly Notices of the Royal Astronomical Society*, 444(4):3738–3755, 2014.

Zhi-Jia Tian, Xiao-Wei Liu, Hai-Bo Yuan, Bing-Qiu Chen, Mao-Sheng Xiang, Yang Huang, Chun Wang, Hua-Wei Zhang, Jin-Cheng Guo, Juan-Juan Ren, Zhi-Ying Huo, Yong Yang, Meng Zhang, Shao-Lan Bi, Wu-Ming Yang, Kang Liu, Xian-Fei Zhang, Tan-Da Li, Ya-Qian Wu, and Jing-Hua Zhang. Binary star fractions from the lamost dr4. *Research in Astronomy and Astrophysics*, 18(5):052, may 2018. doi: 10.1088/1674-4527/18/5/52. URL `https://dx.doi.org/10.1088/1674-4527/18/5/52`.

Jarrod R Hurley, Christopher A Tout, and Onno R Pols. Evolution of binary stars and the effect of tides on binary populations. *Monthly Notices of the Royal Astronomical Society*, 329 (4):897–928, 2002.

RF Webbink. Double white dwarfs as progenitors of r coronae borealis stars and type i supernovae. *The Astrophysical Journal*, 277:355–360, 1984.

Nicholas C Stone, Brian D Metzger, and Zoltán Haiman. Assisted inspirals of stellar mass black holes embedded in agn discs: solving the 'final au problem'. *Monthly Notices of the Royal Astronomical Society*, 464(1):946–954, 2017.

Bence Kocsis. Dynamical formation of merging stellar-mass binary black holes. In *Handbook of Gravitational Wave Astronomy*, pages 1–44. Springer, 2022.

Subrahmanyan Chandrasekhar. Dynamical friction. i. general considerations: the coefficient of dynamical friction. *Astrophysical Journal*, 97:255–262, 1943.

Douglas C Heggie. Binary evolution in stellar dynamics. *Monthly Notices of the Royal Astronomical Society*, 173(3):729–787, 1975.

JG Hills. The effect of low-velocity, low-mass intruders (collisionless gas) on the dynamical evolution of a binary system. *Astronomical Journal (ISSN 0004-6256), vol. 88, Aug. 1983, p. 1269-1283.*, 88:1269–1283, 1983.

Gerald D Quinlan. The time-scale for core collapse in spherical star clusters. *arXiv preprint astro-ph/9606182*, 1996.

Philip Carl Peters. Gravitational radiation and the motion of two point masses. *Physical Review*, 136(4B):B1224, 1964.

ES Light, RE Danielson, and M Schwarzschild. The nucleus of m31. *The Astrophysical Journal*, 194:257–263, 1974.

Walter Dehnen. A family of potential–density pairs for spherical galaxies and bulges. *Monthly Notices of the Royal Astronomical Society*, 265(1):250–256, 1993.

Iskren Y Georgiev and Torsten Böker. Nuclear star clusters in 228 spiral galaxies in the hst/wfpc2 archive: catalogue and comparison to other stellar systems. *Monthly Notices of the Royal Astronomical Society*, 441(4):3570–3590, 2014.

Rubén Sánchez-Janssen, Patrick Côté, Laura Ferrarese, Eric W Peng, Joel Roediger, John P Blakeslee, Eric Emsellem, Thomas H Puzia, Chelsea Spengler, James Taylor, et al. The next generation virgo cluster survey. xxiii. fundamentals of nuclear star clusters over seven decades in galaxy mass. *The Astrophysical Journal*, 878(1):18, 2019.

Henry C Ferguson and Allan Sandage. The spatial distributions and intrinsic shapes of dwarf elliptical galaxies in the virgo and fornax clusters. *The Astrophysical Journal*, 346:L53–L56, 1989.

Mayte Alfaro-Cuello, Nikolay Kacharov, Nadine Neumayer, Nora Luetzgendorf, Anil C Seth, Torsten Boeker, Sebastian Kamann, Ryan Leaman, Glenn van de Ven, Paolo Bianchini, et al. A deep view into the nucleus of the sagittarius dwarf spheroidal galaxy with muse. i. data and stellar population characterization. *The Astrophysical Journal*, 886(1):57, 2019.

HH Loose, E Kruegel, and A Tutukov. Bursts of star formation in the galactic centre. *Astronomy and Astrophysics*, 105:342–350, 1982.

E Schinnerer, T Böker, E Emsellem, and D Downes. Bar-driven mass build-up within the central 50 pc of ngc 6946. *Astronomy & Astrophysics*, 462(3):L27–L30, 2007.

Iskren Y Georgiev, Michael Hilker, Thomas H Puzia, Paul Goudfrooij, and Holger Baumgardt. Globular cluster systems in nearby dwarf galaxies–ii. nuclear star clusters and their relation to massive galactic globular clusters. *Monthly Notices of the Royal Astronomical Society*, 396 (2):1075–1085, 2009.

Giacomo Fragione and Joseph Silk. Repeated mergers and ejection of black holes within nuclear star clusters. *Monthly Notices of the Royal Astronomical Society*, 498(4):4591–4604, 2020.

Nicola Giacobbo, Michela Mapelli, and Mario Spera. Merging black hole binaries: the effects of progenitor's metallicity, mass-loss rate and eddington factor. *Monthly Notices of the Royal Astronomical Society*, 474(3):2959–2974, 2018.

Nicola Giacobbo and Michela Mapelli. The progenitors of compact-object binaries: impact of metallicity, common envelope and natal kicks. *Monthly Notices of the Royal Astronomical Society*, 480(2):2011–2030, 2018.

Nicola Giacobbo and Michela Mapelli. The impact of electron-capture supernovae on merging double neutron stars. *Monthly Notices of the Royal Astronomical Society*, 482(2):2234–2243, 2019.

Nicola Giacobbo and Michela Mapelli. Revising natal kick prescriptions in population synthesis simulations. *The Astrophysical Journal*, 891(2):141, 2020.

Xisco Jiménez-Forteza, David Keitel, Sascha Husa, Mark Hannam, Sebastian Khan, and Michael Pürrer. Hierarchical data-driven approach to fitting numerical relativity data for nonprecessing binary black holes with an application to final spin and radiated energy. *Physical Review D*, 95(6):064024, 2017.

Carlos O Lousto, Yosef Zlochower, Massimo Dotti, and Marta Volonteri. Gravitational recoil from accretion-aligned black-hole binaries. *Physical Review D*, 85(8):084015, 2012.

Fabio Antonini, Mark Gieles, and Alessia Gualandris. Black hole growth through hierarchical black hole mergers in dense star clusters: implications for gravitational wave detections. *Monthly Notices of the Royal Astronomical Society*, 486(4):5008–5021, 2019.

Mark Den Brok, Reynier F Peletier, Anil Seth, Marc Balcells, Lilian Dominguez, Alister W Graham, David Carter, Peter Erwin, Henry C Ferguson, Paul Goudfrooij, et al. The hst/acs coma cluster survey–x. nuclear star clusters in low-mass early-type galaxies: scaling relations. *Monthly Notices of the Royal Astronomical Society*, 445(3):2385–2403, 2014.

Miloš Milosavljević and David Merritt. The final parsec problem. *AIP Conference Proceedings*, 686(1):201–210, 2003.